



RESEARCH ARTICLE

10.1002/2015JC011154

Spatial and temporal variations of the seasonal sea level cycle in the northwest Pacific

Xiangbo Feng^{1,2,3}, Michael N. Tsimplis², Marta Marcos⁴, Francisco M. Calafat², Jinhai Zheng³, Gabriel Jordà⁴, and Paolo Cipollini²¹Department of Meteorology, University of Reading, Reading, UK, ²National Oceanography Centre, Southampton, UK,³State Key Laboratory of Hydrology-Water Resources and Hydraulic Engineering, Hohai University, Nanjing, China,⁴IMEDEA (CSIC-UIB), Esporles, Spain

Key Points:

- Seasonal sea level variations observed by tide gauges and AVISO are identified and compared
- Contributions of IB effect and steric height vary with regions
- Wind stress and surface currents well explain the long-term changes in seasonal sea level cycle

Supporting Information:

- Supporting Information S1

Correspondence to:

X. Feng,
xiangbo.feng@reading.ac.uk

Citation:

Feng, X., M. N. Tsimplis, M. Marcos, F. M. Calafat, J. Zheng, G. Jordà, and P. Cipollini (2015), Spatial and temporal variations of the seasonal sea level cycle in the northwest Pacific, *J. Geophys. Res. Oceans*, 120, 7091–7112, doi:10.1002/2015JC011154.

Received 22 JUL 2015

Accepted 6 OCT 2015

Accepted article online 9 OCT 2015

Published online 31 OCT 2015

The copyright line for this article was changed on 05 NOV 2015 after original online publication.

© 2015. The Authors.

This is an open access article under the terms of the Creative Commons Attribution-NonCommercial-NoDerivs License, which permits use and distribution in any medium, provided the original work is properly cited, the use is non-commercial and no modifications or adaptations are made.

Abstract The seasonal sea level variations observed from tide gauges over 1900–2013 and gridded satellite altimeter product AVISO over 1993–2013 in the northwest Pacific have been explored. The seasonal cycle is able to explain 60–90% of monthly sea level variance in the marginal seas, while it explains less than 20% of variance in the eddy-rich regions. The maximum annual and semiannual sea level cycles (30 and 6 cm) are observed in the north of the East China Sea and the west of the South China Sea, respectively. AVISO was found to underestimate the annual amplitude by 25% compared to tide gauge estimates along the coasts of China and Russia. The forcing for the seasonal sea level cycle was identified. The atmospheric pressure and the steric height produce 8–12 cm of the annual cycle in the middle continental shelf and in the Kuroshio Current regions separately. The removal of the two attributors from total sea level permits to identify the sea level residuals that still show significant seasonality in the marginal seas. Both nearby wind stress and surface currents can explain well the long-term variability of the seasonal sea level cycle in the marginal seas and the tropics because of their influence on the sea level residuals. Interestingly, the surface currents are a better descriptor in the areas where the ocean currents are known to be strong. Here, they explain 50–90% of interannual variability due to the strong links between the steric height and the large-scale ocean currents.

1. Introduction

The seasonal cycle, and more specifically its annual and semiannual components, dominates the nontidal variability of sea level in many regions of the ocean. Because the seasonal variability is very energetic for monthly sea level records and also it is autocorrelated, this signal is normally removed from the estimation of trends of mean sea level. However, this does not hide the practical significance of the seasonal cycle. Coastal infrastructure is more vulnerable at the time when the seasonal sea level cycle is at its highest [Tsimplis and Shaw, 2010; Dangendorf et al., 2013a; Torres and Tsimplis, 2014], and the decadal increases in the seasonal cycle will make the vulnerability of the coastal areas even higher. The seasonal changes in stratification, which are seen in the seasonal sea level cycle, can cause significant seasonal changes in tides [Kang et al., 2002; Müller et al., 2014], leading to the prediction of tides and extremes more complicated. Furthermore, the seasonal sea level cycle is firmly regulating the seawater-freshwater balance both under the ground [Michael et al., 2005] and at the river estuaries [Anderson and Lockaby, 2012], and it acts as a key factor determining the seawater intrusion. Therefore, obtaining good physical understanding of the processes involved in determining the seasonal sea level cycle and its spatial and temporal changes enables us to assess the extent of future changes in climate that will impact on the coastal ocean environments.

The gravitational forcing contributes very little (in millimeter) to the observed seasonal sea level cycle [Pugh and Woodworth, 2014]. Seasonality in meteorological, oceanographic, and hydrological processes is considered to force the seasonal sea level cycle, but the contribution of each factor varies spatially and temporally [Plag and Tsimplis, 1999; Marcos and Tsimplis, 2007; Hünicke and Zorita, 2008; Vinogradov et al., 2008; Torres and Tsimplis, 2012; Dangendorf et al., 2013b; Wahl et al., 2014]. Notably, temporal changes in the seasonal sea level cycle may be caused by the sea level components which are not the dominant ones. Therefore, mapping the seasonal sea level cycle, identifying the dominant components regionally and furthermore identifying the forcing of its temporal changes is very important in order to understand the physics of the sea level variability at the seasonal frequencies.

On the basis of tide gauge data, *Tsimplis and Woodworth* [1994] mapped the features of the seasonal sea level cycle in coastal waters, showing spatial variability but also regional coherence. Satellite radar altimetry has the capability of monitoring the sea level variations with a better spatial coverage, and the native altimetric along-track data are often gridded for further use of analysis and visualization. *Chen et al.* [2000] explored the estimations of the seasonal cycle in open oceans using gridded altimeter measurements. However, at the continental coasts the altimetry was found to significantly underestimate the annual level cycle [*Han and Huang*, 2008; *Vinogradov and Ponte*, 2010]. This underestimation is normally caused by a combination of data flagging (in turn due to contamination of the altimetric waveforms and/or inadequacy of some of the corrections such as the one compensating for path delay due to water vapor) and data filtering in the last 20–30 km from the coasts. For the gridded altimeter data, the mapping procedure additionally tends to smooth the characteristics of the local phenomena of sea level that are captured by the tide gauges. For each region, it is vital to clearly identify the uncertainty of the altimeter products in estimating the seasonal sea level before using their results into other fields. It is worth noting that considerable research efforts are being put into improving the along-track altimetry in the coastal zone [*Vignudelli et al.*, 2011]. The latest coastal altimetry products reprocessed with improved techniques allow a better representation of sea level variability near the coasts [*Passaro et al.*, 2015] but those products are not yet available for all the past missions and coastal areas and therefore time series are limited.

The stability of the seasonal sea level cycle with time has also been studied for a few regions where long-term tide gauge records exist. The annual cycle amplitude was found to exhibit decadal variations between 1 and 20 cm in the European coasts [*Plag and Tsimplis*, 1999; *Barbosa et al.*, 2008; *Hünicke and Zorita*, 2008; *Dangendorf et al.*, 2013b], the Mediterranean Sea [*Marcos and Tsimplis*, 2007], the Caribbean Sea [*Torres and Tsimplis*, 2012], and the South China Sea [*Amiruddin et al.*, 2015]. Interestingly, the annual cycle amplitude along the U.S. Gulf coast was recently reported to have increased by 20–30% since 1990s, and the sea surface air temperature was argued as an indicator for the increase [*Wahl et al.*, 2014]. These studies are all based on the traditional annual cycle definitions, assuming that both amplitude and frequency of the annual cycle are constant within each time segment of assessments but that they are allowed to change over different segments. Consequently, there is a possibility that the interannual or even lower-frequency variability in the monthly values may be treated as part of the annual cycle signal if the length of assessment windows is not appropriate. An alternative method, the modulated annual cycle that allows the annual cycle parameters to change instantaneously, was introduced to the climate analysis by *Wu et al.* [2008]. Based on this concept, some reconstruction products have been made to recover the high and low-frequency signals in sea level [*Hamlington et al.*, 2011, 2012].

The northwest Pacific is a region where both oceanographic and atmospheric dynamics (e.g., the western boundary currents, the monsoon, and typhoons) are known to have strong impacts on the sea surface processes. The areas studied here are of particular interest also because they are heavily populated areas where intensive anthropogenic activities were found to have significantly changed the coastal geomorphology [*Wang et al.*, 2014, and references therein]. *Marcos et al.* [2012] identified the spatial and temporal variations of mean sea level in the marginal seas of this region and associated them with the large-scale climatic variability. *Feng et al.* [2015] explored the long-term changes in tidal signals and proposed them as the consequences of the anthropogenic activities. These sea level components were suggested to consequently alter the occurrence of extremes [*Feng and Tsimplis*, 2014]. However, the seasonal cycle, as a crucial component in sea level, has not been systematically studied over the whole region of the northwest Pacific. The dynamics behind the spatial and temporal variations remain unrevealed.

This paper provides a regional investigation on the seasonal sea level cycle over the northwest Pacific, by using publically accessible data sets, which include tide gauge records, gridded satellite altimetry data, and atmospheric and oceanic reanalysis. Four questions are addressed. First, what are the spatial features of the seasonal sea level cycle in this region; second, to what extent can gridded satellite altimetry product estimate the coastal seasonal sea level cycle; third, how much do the seasonal signals change with time; and fourth, what are the causes for the seasonal sea level oscillations and for their long-term variability as well, and to what extent can each of the contributors explain the variability.

The paper is structured as follows. In section 2, the data processing of sea level observations and atmospheric and oceanic climate reanalysis used are described together with the methodologies. In section 3, spatial features of the seasonal sea level cycle are investigated, and harmonic parameters estimated from

tide gauges and gridded altimetry data are compared. Temporal variability of the seasonal cycle is also addressed in this section. In section 4, mechanisms for the spatial and temporal changes of the seasonal sea level cycle are explored, including the atmosphere pressure loading, the ocean thermal expansion/contraction and freshwater content, the wind stress, and the sea surface currents. Finally, the conclusions are given in section 5.

2. Data and Methodology

2.1. Sea Level Observational Records

Monthly sea level data (η) recorded at 120 tide gauges in the northwest Pacific were obtained from the Permanent Service for Mean Sea Level [Holgate *et al.*, 2013]. Locations and numbering of the 120 tide gauge stations are provided in Figure 1a. Tide gauges are classified into six subregions: the east of the South China Sea (SCS-E) (station number: 1–14), the west of the South China Sea (SCS-W) (station number: 15–39), the East China Sea (ECS) (station number: 40–61), the Sea of Japan (SoJ) (station number: 62–89), the northeast coasts of Japan (Japan-NE) (station number: 90–105), and the southeast coasts of Japan (Japan-SE) (station number: 106–115). There are two stations on the coasts of the Sea of Okhotsk (station number: 119 and 120) and three stations in the south of Japan (station number: 116–118) where the observed seasonal sea level cycle has different behavior from that at neighboring sites (this will be discussed in subsection 3.3). Thus, these five stations are taken as outliers relative to above six subregions. The data set used spans the period 1900–2013. However, only a few stations have records longer than 50 years (Figure 1b). The minimum record length used in the analysis was 16 years. The data set contains 105 revised local reference records and 15 metric records. The metric records do not contain the information about the benchmark datum contributed by releveling adjustments to a certain level, but they can be useful for studies of the seasonal sea level cycle if they are carefully treated.

The data quality control of tide gauge records performed included the visual checks of time series and the adjustment or removal of values over periods with spurious shifts. Although it is not necessary to know the actual level of the datum for estimating the seasonal cycle, the stability of the datum is still important for assessing the temporal variability of the cycle. Where a record showed datum shifts over different segments these were adjusted to the same reference level by removing their mean values after each segment was detrended. Sea level values that showed obvious jumps or shifts after the known earthquakes were also excluded. Two massive earthquakes were considered, which stroke the Kuril Islands on the 4 October 1994 and the Oshika Peninsula on the 11 March 2011, respectively (www.nodc.noaa.gov/outreach/esm). For individual records, mean values and trends were removed and then plotted into six groups as specified above. In each group, if parts of records show spurious jumps or shifts compared with other members, or go beyond the spreading edges of the ensembles, these records are omitted. Figure 1b gives the period of valid data at each station after the quality control.

Gridded satellite radar altimeter data that cover the northwest Pacific (0–65°N, 100°E–170°E) were also used. The data were produced by SSALTO/DUACS and distributed by AVISO, with support from CNES (<http://www.aviso.altimetry.fr/duacs/>). The data consist of monthly averaged maps of sea level anomalies, corresponding to multimission gridded sea surface height anomaly (including Saral, Cryosat-2, Jason-1&2, T/P, Envisat, GFO, ERS-1&2, and Geosat) with respect to a 21 year mean sea level. The spatial resolution of the gridded altimeter data is $1/4^\circ \times 1/4^\circ$, which permits resolving the sea level related to the mesoscale eddies. Oceanic and atmospheric dynamics are routinely corrected in the mission track data. These include the ocean tide, the pole tide, and the dynamic atmospheric correction (DAC) [Carrère and Lyard, 2003]. Because the inverted barometer (IB) effect (η_{IB}) has been corrected in the AVISO data, we here refer to the monthly sea level records from AVISO as $\eta - \eta_{IB}$.

2.2. Atmospheric Pressure Data and the IB Effect

In the open ocean, the sea level is assumed to isostatically react to the atmospheric pressure loading on the sea surface by the inverted barometer (IB) effect (η_{IB}) [Gill, 1982; Wunsch and Stammer, 1997; Ponte, 2006]. $\eta_{IB} = -1/\rho g(P - P_{ref})$, where ρ and g are the water density and gravity acceleration, respectively, and $P - P_{ref}$ is the fluctuation of sea level pressure P relative to a long-term average P_{ref} over the global ocean [Wunsch and Stammer, 1997; Ponte, 2006]. The consequence of a 1 mbar increase in surface pressure is approximately 1 cm depression of sea level.

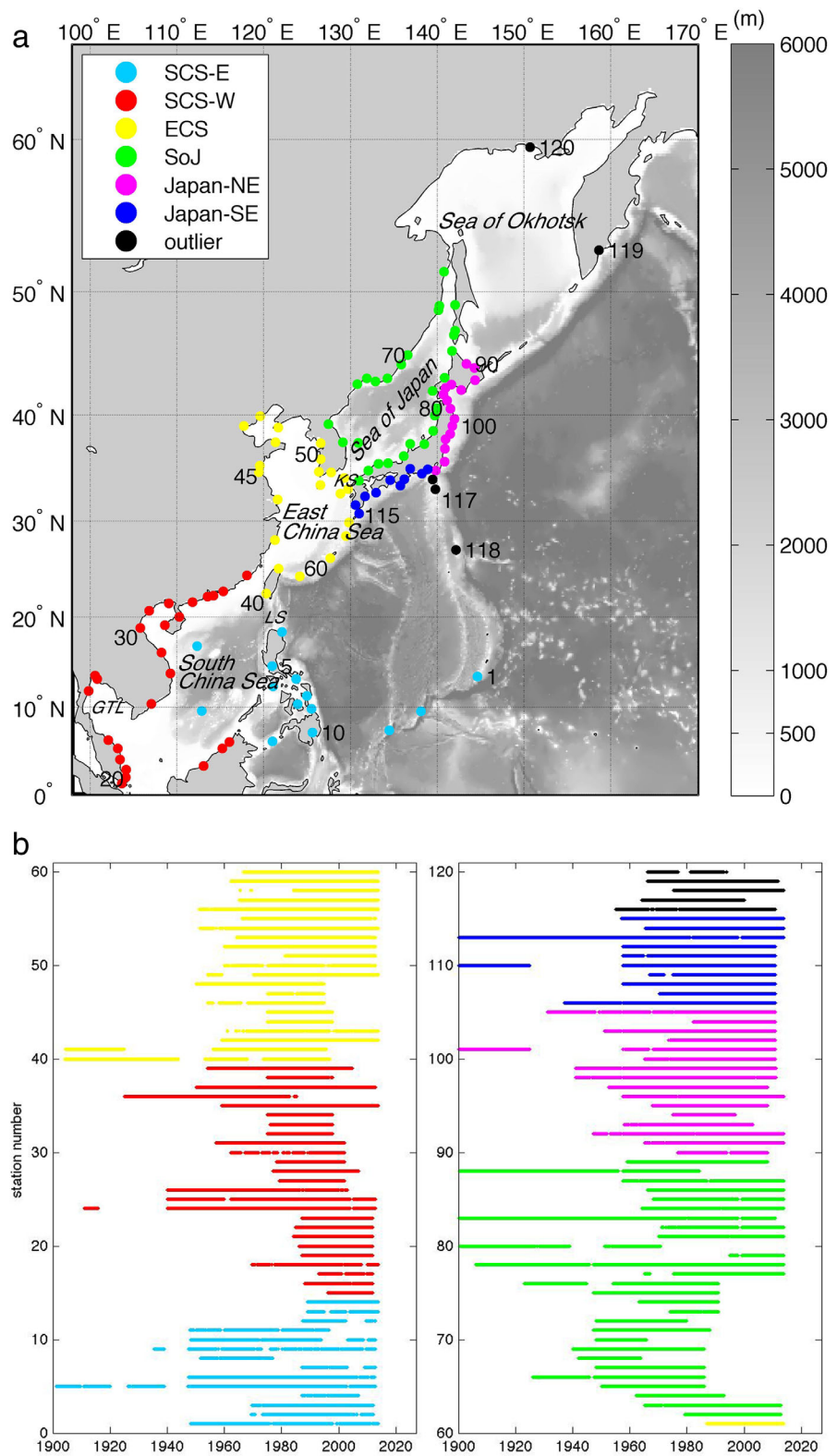


Figure 1. (a) Study areas and locations of 120 tide gauges, and (b) periods of valid η observed from tide gauges. Tide gauges are colored and numbered into six subregions, with five stations treated as outliers (black dots). The six subregions are named as the east of the South China Sea (SCS-E), the west of the South China Sea (SCS-W), the East China Sea (ECS), the Sea of Japan (SoJ), the northeast coasts of Japan (Japan-NE), and the southeast coasts of Japan (Japan-SE). KS, LS, and GTL represent the Korea Strait, the Luzon Strait, and the Gulf of Thailand, respectively.

With respect to the tide gauge records, the monthly sea level pressure data over 1900–2013 were used to calculate η_{IB} closest to the stations. The pressure data were obtained by combining the NOAA’s 20th century reanalysis v2 for the period 1900–2012 [Compo *et al.*, 2011] and the ECMWF-Interim for 2013. Please note that for each tide gauge record η_{IB} is only applied over the periods when the tide gauge has valid data.

For AVISO records, the monthly average of 6 h dynamic atmospheric corrections (DAC) was used as η_{IB} over the sea surface. The DAC data are the sea level variability combining the high-frequency signals (less than 20 days) due to atmospheric wind and pressure forcing and low-frequency signals (more than 20 days) from the static IB correction on the atmospheric pressure. The monthly average of DAC is equivalent to the isostatic IB effect [Pascual *et al.*, 2008]. The DAC data are produced by CLS Space Oceanography Division using the Mog2D model from Legos [Carrère and Lyard, 2003] and distributed by AVISO.

2.3. Ocean Temperature and Salinity Analysis and the Steric Height

The steric height was calculated from the 3-D hydrographic-gridded product EN4.0.2 generated by the UK Met Office Hadley Centre. This product has been generated through the objective analysis of a global quality controlled data set of ocean temperature and salinity profiles, and is provided on a grid with 1° spatial resolution in the horizontal and 42 levels in the vertical [Good *et al.*, 2013] covering the period 1900–2013. The main observational data source is WOD09 [Boyer *et al.*, 2009]. The steric component of seasonal sea level change is mainly due to the water density changes over the thermocline depth [Chen *et al.*, 2000; Vinogradov *et al.*, 2008; Torres and Tsimplis, 2012]. Therefore, the values over the top 500m were used in the calculation of the steric signal.

The steric height (η_{ster}), consisting of thermosteric (η_{thermo}) and halosteric components (η_{halo}), over water depth (H) can be expressed as:

$$\begin{aligned} \eta_{thermo} &= \int_{-H}^0 C \cdot \Delta T dz \\ \eta_{halo} &= \int_{-H}^0 D \cdot \Delta S dz \end{aligned} \tag{1}$$

where ΔT and ΔS are the temperature and salinity fluctuation relative to the mean values over the whole period of study at each layer, and C and D are the thermal expansion and salt compression coefficients, respectively [Tabata *et al.*, 1986]. C and D are defined as

$$\begin{aligned} C &= -\frac{1}{\rho} \frac{\partial \rho}{\partial T} \\ D &= -\frac{1}{\rho} \frac{\partial \rho}{\partial S} \end{aligned} \tag{2}$$

where ρ is the water density, depending on water depth, temperature, and salinity, and is defined by the Joint Panel on Oceanographic Tables and Standards [UNESCO, 1981].

η_{ster} calculated at tide gauge stations or shallow water regions is usually very small and cannot represent the entire seasonal steric signal. Thus we used the values at deep grid points (over 500 m) closest to the sites of interest. This method assumes that the whole steric signal in the deep ocean is transmitted to the coast [Bingham and Hughes, 2012].

We also repeated the above process to calculate η_{ster} based in the 3-D gridded oceanic properties from the Simple Ocean Data Assimilation (SODA), which will be introduced later, in order to explain the mechanisms of the long-term variations of the seasonal sea level cycle.

2.4. Ocean Reanalysis SODA

The sea surface height without the IB effect ($\eta - \eta_{IB}$), 3-D ocean temperature and salinity, the wind stress and the sea surface currents from the Simple Ocean Data Assimilation (SODA) v2.2.4 covering the period 1900–2010 were also used to understand the forcing of the seasonal sea level cycle. The SODA reanalysis is based on the Parallel Ocean Program ocean model [Smith *et al.*, 1992], with $0.25^\circ \times 0.4^\circ$ horizontal resolution and 40 vertical levels, and assimilates oceanic data through an optimal interpolation method every 10 days [Carton *et al.*, 2000]. In the version v2.2.4 [Giese and Ray, 2011], the observations used in the data assimilation scheme only include the ocean temperature and salinity profiles from WOD09 [Boyer *et al.*, 2009] (it is also the main data source for the Met Office Hadley Centre EN4) and sea surface temperature from ICOADS

2.5 [Woodruff *et al.*, 2011]. Thus, SODA is expected to be able to seasonally represent the steric height in sea level. It is worth noting that SODA does not assimilate sea level observations (i.e., from altimetry or tide gauges). The model is forced with atmospheric fields from the NOAA's 20th century reanalysis v2 [Compo *et al.*, 2011] over the period 1871–2010 [Carton and Giese, 2008].

We use SODA for the purpose of identifying the forcing of the seasonal sea level cycle (the method used in estimating the seasonal sea level cycle will be described in the next subsection). To do so, it is necessary to first assess the capability of SODA in describing the observed seasonal sea level cycle in this region. Please note that because SODA does not include the IB effect, in the assessment η_{IB} was excluded both in AVISO data and in tide gauge records, ensuring that the three data sets are all free of the IB effect. Details of the assessment are provided in supporting information. The comparison results are summarized as: (1) the mean seasonal sea level cycle determined by SODA over 1993–2010 is in good agreement with the estimations observed by AVISO over 1993–2013 in most areas, with some discrepancies for annual amplitudes below 3–6 cm and mainly occurring at the coastal regions (supporting information Figures S1 and S2); (2) the interannual variability of the seasonal sea level cycle over 1900–2010 from SODA has significant correlation with the results observed at most of the tide gauge records (in 96 of 120), with $R = 0.59$ and 0.58 on average for annual and semiannual amplitudes, respectively, and the worse representation of SODA is mainly in the north of East China Sea and the north of the Sea of Japan where the tide gauge records are relatively short (supporting information Figure S3); and (3) when the regional average is concerned, SODA can well represent the interannual variability of the seasonal sea level cycle for each subregion (supporting information Figure S4), with correlation $R = 0.61$ and 0.57 on average for annual and semiannual amplitudes against tide gauge observations. Thus, we conclude that SODA reproduces the seasonal sea level cycle in the area of study with a reasonable accuracy and we will use it in the characterization of the forcing mechanisms that determine the seasonal cycle.

It should be kept in mind that discrepancies of SODA still exist in the seasonal sea level cycle estimations. This can be due to many different aspects of SODA, such as the quality of atmospheric forcing, the low resolutions of the model at coasts, the nonconserving global water mass [Tamisiea *et al.*, 2010], or the nonconserving budgets in the ocean data assimilation procedure [Haines *et al.*, 2012]. More efforts are needed to interpret the skills of SODA, but this is not the scope of this paper.

2.5. Regression Model for Seasonal Cycle

The harmonic parameters of the annual and semi-annual cycles were estimated through least squares fitting to the monthly records by the following equation:

$$\eta(t) = \beta_0 + A_a \cos\left(\frac{2\pi}{12}(t - \phi_a)\right) + A_{sa} \cos\left(\frac{2\pi}{6}(t - \phi_{sa})\right) \quad (3)$$

where $\eta(t)$ is the monthly mean value of sea level at time t (in units of months and corresponding to the middle of January), β_0 is the estimated mean value, and A_a and A_{sa} are the annual and semiannual amplitudes corresponding to the phase lags of ϕ_a and ϕ_{sa} , respectively. The significance of the estimated harmonic parameters was tested at 95% confidence level by assuming the regression errors are normally distributed. Note that all the monthly records used in the analysis were detrended over the period before being fitted by equation (3).

The mean seasonal cycle for each sea level record was estimated on the basis of equation (3) using the data over the whole period. The temporal variability of the seasonal cycle was also estimated on the basis of applying equation (3) for 5 year segments shifted year-by-year. The 5 year length of data segment was chosen as suggested by Tsimplis and Woodworth [1994] as a period over which most records provide stable estimates for the seasonal cycle.

We applied this method to different sea level components, the wind stress, and the sea surface currents, to diagnose the forcing mechanisms of the seasonal sea level cycle. In estimating the temporal variability of the seasonal cycle for the wind stress and the sea surface currents, the two variables as 2-D vectors are equally divided into 18 sections (0–180° relative to the east anticlockwise by 10°) to get their values at different directions. This process permits us to distinguish the vectors with the direction that have the best correlations with the seasonal sea level variations.

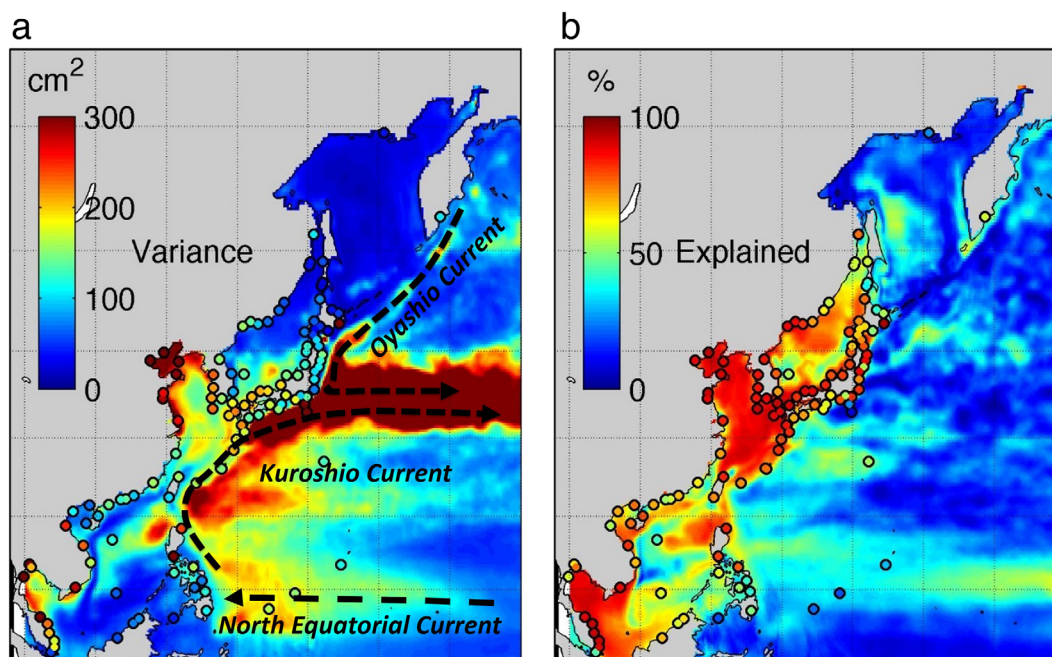


Figure 2. (a) Variance of η observed from tide gauges and AVISO, and (b) percentage of the variance explained by the seasonal cycle. Schematic routes of the Oyashio, the Kuroshio, and the North Equatorial Currents are indicated by the black dashed lines in Figure 2a, which are estimated using the altimeter data distributed by AVISO.

3. Seasonal Sea Level Cycle From Observations

3.1. Monthly Sea Level Variations

The monthly variances of η from tide gauges and AVISO are shown in Figure 2a. Note that η from AVISO is obtained by adding η_{IB} (DAC data) back to $\eta - \eta_{IB}$ (AVISO sea level records). The variance exceeds 300 cm^2 in the north of the East China Sea and in regions with strong western boundary currents, i.e., the Kuroshio Extension and the south Oyashio Currents. Values of $150\text{--}200 \text{ cm}^2$ are found in the East China Sea, the Luzon Strait, the Gulf of Thailand, and the area of the Equatorial Current.

Figure 2b shows the percentage of variance explained by the seasonal cycle regression model of equation (3). The regression model explains 60–90% of the variance in the vast majority of areas of the marginal seas over the continental shelf, except in the Sea of Okhotsk where sea ice usually exists in cold seasons [Parkinson *et al.*, 1999]. In the open ocean, the percentage of variance explained by the seasonal cycle is very low, except in a zonal band ($10^\circ\text{N}\text{--}20^\circ\text{N}$) and in the west of the ocean interior where 40–50% of sea level variance can be attributed to the seasonal cycle. It is worth noting that in the regions of the Kuroshio Extension and the south Oyashio Currents, where the sea level variance is maximum (Figure 2a), the seasonal cycle captures less than 20% of variance (Figure 2b). The low representativeness of the seasonal cycle in the open ocean can be interpreted by the presence of eddies which have the strong signature in sea level (and thus induce high variance in sea level observations) but which usually have much irregular seasonal variations. In fact, this region has been identified as the region with the richest mesoscale eddies in the world [Chelton *et al.*, 2011].

The sea level variance observed by AVISO at the closest points to tide gauges is lower than that observed by tide gauges at 96 of the 120 stations. The difference of variance (AVISO—tide gauges) is -31 cm^2 on average (21% of variance determined by tide gauges). The largest discrepancies occur in the north of the Philippines and at the west of the South China Sea (Figure 2a). When the period of AVISO (1993–2013) is considered, there are 103 tide gauge records having valid data over the period. AVISO is then found to underestimate the sea level variance again at 64 of the 103 stations by overall -16 cm^2 (11% of variance by tide gauges). Thus, we conclude that AVISO underestimates the coastal sea level variance at most of stations disregarding the period.

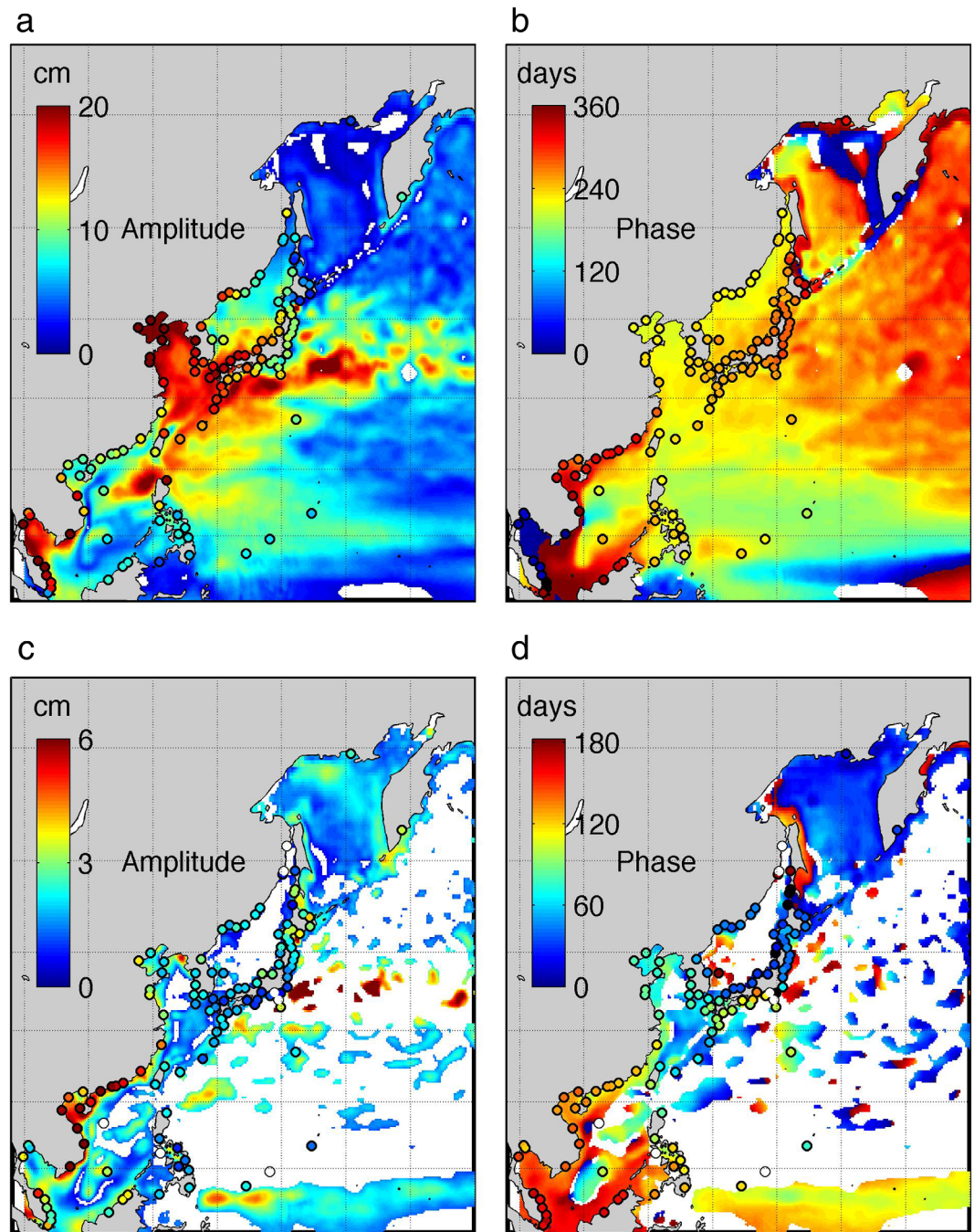


Figure 3. Mean (a) A_a , (b) ϕ_a , (c) A_{sa} , and (d) ϕ_{sa} of η from tide gauges and AVISO. Blank areas and circles indicate the estimates of the annual or semiannual cycle parameters that are not passing the significance test at 95% confidence level.

In the estimations, the annual and semiannual cycle parameters in equation (3) are assumed to be constant during the whole period of records. Actually, as we will discuss later, they could change in time. Thus, we cannot rule out the possibility that the sea level variance accounted by the seasonal cycle and the resulting percentages as indicated above may change when different periods of time are considered.

3.2. Mean Seasonal Sea Level Cycle

The annual cycle of η is significant at all tide gauge records and in most areas (Figures 3a and 3b). The values of A_a exceed 15cm in the East China Sea, the south of Japan, the areas of the Kuroshio Current, the Luzon Strait, and the Gulf of Thailand. A_a is less than 3 cm or becomes statistically insignificant in the

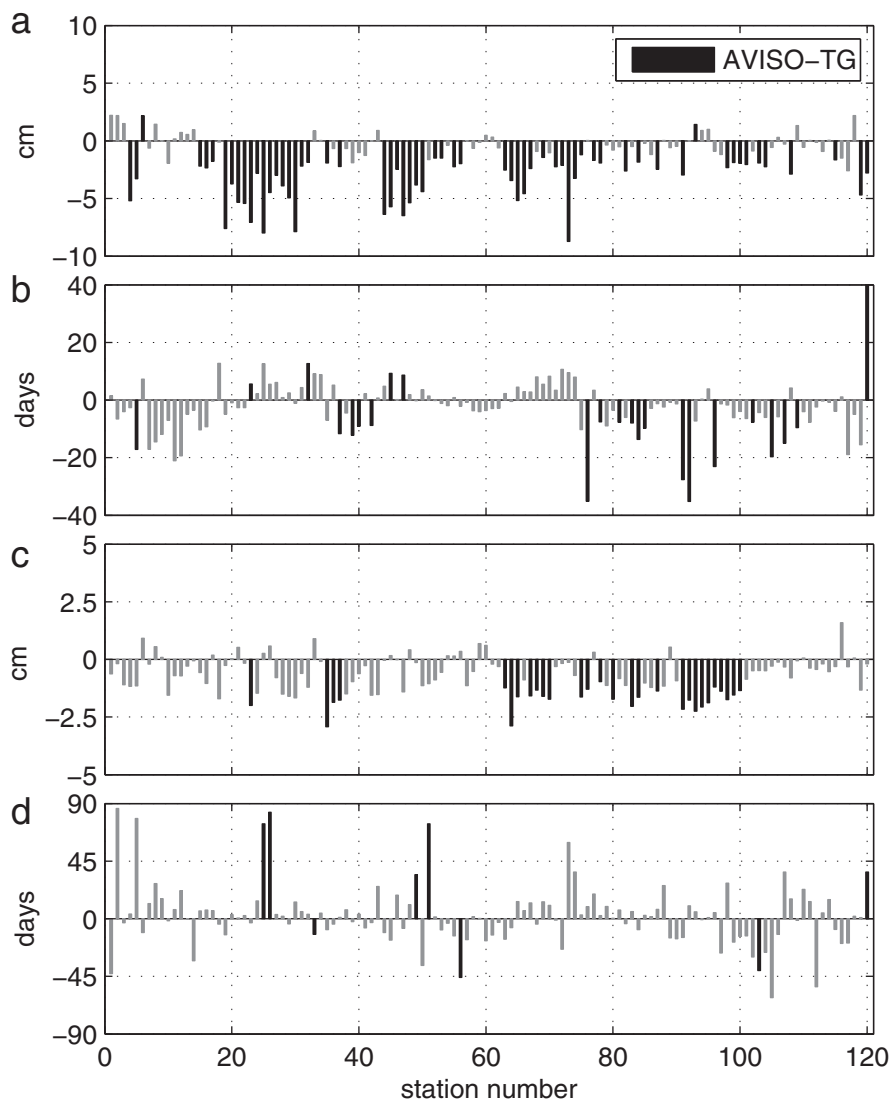


Figure 4. Differences of mean (a) A_a , (b) ϕ_a , (c) A_{sa} , and (d) ϕ_{sa} of η determined by tide gauges and AVISO at the closest points to tide gauges (TG) (AVISO—tide gauges). Black bars indicate the differences that pass the significance test, i.e., error bars of two estimated values (one from AVISO and the other from tide gauges) used in comparison do not overlap, while gray bars indicate the insignificant differences.

equator area ($0\text{--}10^\circ\text{N}$) and the Sea of Okhotsk. The highest A_a (29 ± 1 cm) occurs at the north of the East China Sea (station number: 47 and 48). The annual phase ϕ_a is in December–January in the equator area, while it changes to August–November when heading to north. ϕ_a is not uniform in each basin, except in the East China Sea.

The semiannual cycle is significant at most of tide gauge records (113 of 120), in the equator area and in most areas of marginal seas, except in the Sea of Japan (Figures 3c and 3d). A_{sa} has the highest values of 5–7 cm in the northwest of the South China Sea and in the Kuroshio Extension area. ϕ_{sa} is changing from January to May (or July–November) when heading to south, and the direction of ϕ_{sa} change is in opposite to that of ϕ_a change (Figure 3b).

The comparisons of the annual and semiannual parameters derived from AVISO and tide gauge measurements are shown in Figure 4. The differences are regarded as significant if the error bars of the two compared values do not overlap. At the points closest to tide gauges, AVISO significantly underestimates A_a at 59 of the 120 stations by 2–9 cm, with 3.5 cm on average (25% of tide gauges estimates), and overestimates at two stations (station number: 6 and 93) by 1.4 and 2.2 cm (37% and 42% of tide gauge estimates) (Figure 4a). Large underestimations of 5–8 cm ($\sim 40\%$ of tide gauges values) are found in the west of the

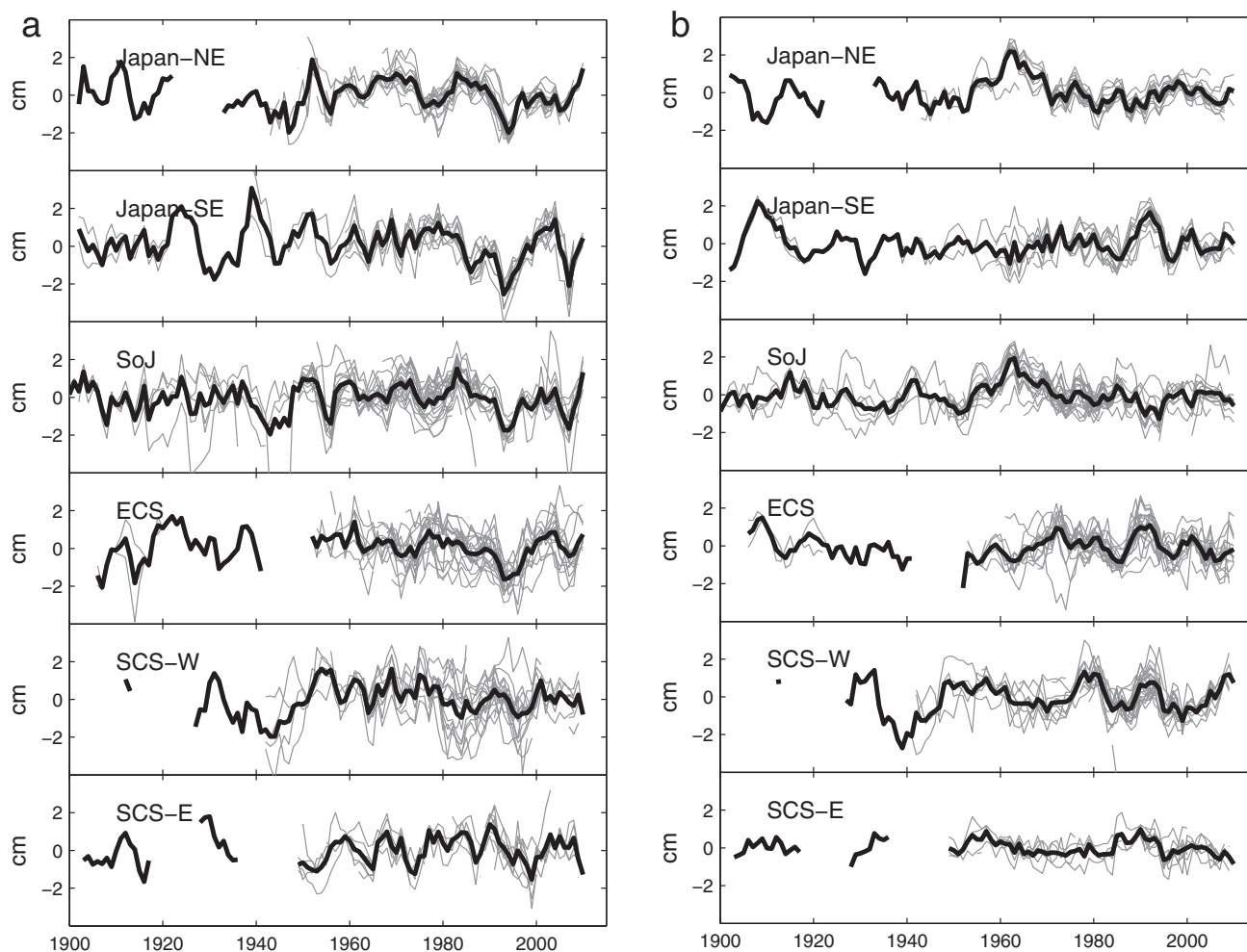


Figure 5. Time series of the anomaly of (a) A_a and (b) A_{sa} of η determined from tide gauges, which are grouped by six subregions as specified in Figure 1. Bold black line is plotted for the regional ensemble average of individual anomalies in each subregion. Note that anomaly is produced by removing the mean value of A_a or A_{sa} from each series.

South China Sea, the East China Sea, and the Sea of Japan. Meanwhile, ϕ_a derived from AVISO is significantly advanced by 10–35 days at 18 stations and delayed by 5–12 days at 4 stations (Figure 4b). The semi-annual cycle is detectable at 113 stations for tide gauge measurements but only detectable at the corresponding AVISO points for 87 stations. AVISO underestimates A_{sa} by 1–3 cm (60%) at 28 of the 87 stations, while discrepancies of ϕ_{sa} occur at only eight stations when the error bars are considered (Figures 4c and 4d).

The discrepancies of the seasonal sea level cycle estimated from AVISO still remain when the common period (1993–2013) is used at tide gauge records for the comparisons. We also found that the differences of harmonic parameters derived from AVISO and tide gauges can well explain the discrepancies of the sea level variance in most of the coastal areas, which have been identified in subsection 3.1. This indicates that the underestimation of the seasonal cycle amplitudes is consistent with the errors of the sea level variance. Therefore, we confirm that the discrepancies of sea level seasonality identified between the two data sets are real and are not due to the methods used in the estimation.

3.3. Temporal Variability of the Seasonal Sea Level Cycle

The temporal variability of the seasonal sea level cycle is produced by fitting equation (3) into a 5 year segment of tide gauge records (η) with year-by-year shifting. Figure 5 shows the interannual variations of the seasonal sea level amplitudes with respect to their own mean amplitudes for each station in the six subregions (gray lines in the figure). The temporal changes for five outlier stations (station number: 116–120) are provided in supporting information (supporting information Figure S5), and at these stations the seasonal

sea level cycle shows different temporal variability in relation to the six subregions. Regional averages of the temporal changes in the seasonal cycle are obtained by averaging all seasonal cycle amplitude anomalies in one subregion (black bold lines in Figure 5).

The annual and semiannual sea level cycles are not constant in time (Figure 5). The range between maximum and minimum A_a at individual stations usually varies from 2 to 8.6 cm, with an average of 4.2 cm (33% of their maximum amplitudes). The largest ranges of 20.4 and 16.5 cm are observed at two outliers in the south of Japan (station number: 116 and 117, see supporting information Figure S5). In spite of apparent regional features, the interannual variability of A_a also shows some consistency among regions. In particular, the significant change by ~ 4 cm for regional averages of A_a in the 1990's was present in all the regions. The range of A_{sa} differences over time is 1–7 cm at individual stations, with an average of 3.3 cm (75% of their maximum amplitudes). The magnitudes of temporal changes in the regional averages of A_{sa} are much smaller than those of A_a . The consistency of the interannual variability of A_{sa} between different subregions is only found in the North East of Japan and the Sea of Japan.

4. Forcing of the Seasonal Sea Level Cycle

4.1. The IB Effect and the Steric Height

4.1.1. The IB Effect (η_{IB})

The mean seasonal sea level cycle of η_{IB} over 1993–2013 is mapped in Figure 6. η_{IB} produces a significant annual sea level cycle over the whole area of study, except in small areas in the Sea of Okhotsk and the central middle-latitude (30–40°N) of Pacific. The annual cycle of η_{IB} exhibits the largest A_a (~ 12 cm) in the middle of the continental shelf, i.e., the north of the East China Sea (Figure 6a). η_{IB} has a uniform ϕ_a (July) over most areas, except in the north central Pacific (35–60°N) where A_a is small and where ϕ_a varies by ~ 6 months (Figure 6b). The origin of the annual cycle of η_{IB} is linked with the strong seasonal variations of the air pressure at high latitudes due to the radiational heating [Yashayaev and Zveryaev, 2001; Gabler et al., 2008].

The atmospherically induced semiannual sea level cycle is only distinguishable at the midlatitudes (30–50°N) of the north Pacific and the west of the South China Sea (Figure 6c). The maximum A_{sa} of ~ 3 cm are located at the center of middle-to-high latitudes (around 43°N and 170°E), but the values are less than 1 cm in most marginal seas. ϕ_{sa} is always in January or July, except in the Gulf of Thailand (Figure 6d).

The interannual variability of the seasonal sea level cycle due to η_{IB} over the same periods of tide gauge records was also calculated by using the long-term atmospheric pressure data. Compared to η , η_{IB} for tide gauge records has very limited interannual variability (less than 3 cm) both in A_a and in A_{sa} . The ranges between maximum and minimum A_a of η_{IB} at individual stations over time are up to 2.4 cm in the north of the East China Sea (station number: 48) and 2.7 cm in the Sea of Okhotsk (station number: 120). The weak impact of η_{IB} on the long-term changes of the seasonal sea level cycle is also revealed in the regional averages (see the supporting information Figure S6).

4.1.2. The Steric Height (η_{ster})

The mean seasonal cycle of η_{ster} derived from EN4 over 1993–2013 is shown in Figure 7. The annual cycle of η_{ster} is significant in the whole area of study, with larger A_a at the midlatitudes and along the Kuroshio Current. The strongest signal with A_a of 12–14 cm is found in the East China Sea, the east of the Sea of Japan, and the east of Japan. ϕ_a keeps homogeneous (\sim September) in the north but it gradually shifts to January near the equator. The annual cycle in η_{ster} is primarily determined by η_{thermo} . A_a of η_{halo} was found to be usually less than 1 cm (not shown here). This is in agreement with the results by Vinogradov et al. [2008].

The semiannual cycle of η_{ster} is statistically significant in the tropics and the north marginal seas (Figure 7c). The largest A_{sa} of 3 cm is found in the east of Philippines and around the north of Japan. ϕ_{sa} shifts quickly with different areas (Figure 7d). The semiannual cycle in η_{ster} is also mainly caused by η_{thermo} .

The interannual variability of the seasonal cycle in η_{ster} at locations at least 500 m deep and closest to tide gauges was also estimated. The ranges of temporal changes of A_a and A_{sa} in η_{ster} are close to those as observed in η . However, there are only 32 (24) of the 120 stations where the interannual variability of A_a (A_{sa}) between η_{ster} and η is significantly correlated (at 95% confidence level). There is no change for the correlations when η_{IB} is removed from the observed η (i.e., $\eta - \eta_{IB}$), confirming the conclusion drawn above that

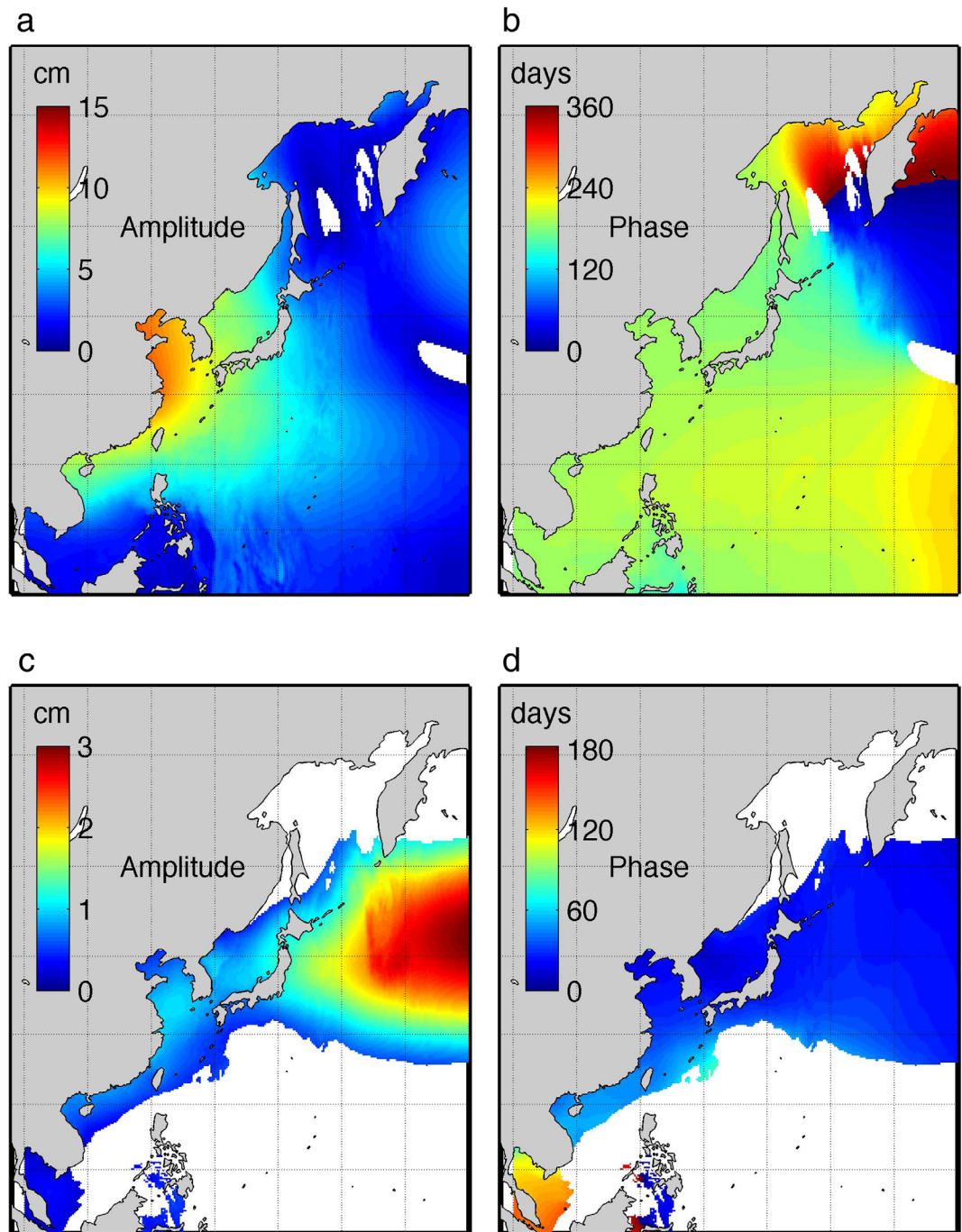


Figure 6. Mean (a) A_a , (b) ϕ_a , (c) A_{sa} , and (d) ϕ_{sa} for η_{IB} derived from DAC data over 1993–2013. Blank areas indicate the estimates of the annual or semiannual cycle parameters that are not passing the significance test at 95% confidence level. Please note that the scales of amplitudes here are different from those in Figure 3.

η_{IB} has very limited influence on the long-term variability of the seasonal sea level cycle. The un-robust relationship between η and η_{ster} for their seasonal cycles can also be evidenced by the mismatching of their regional averages (see the supporting information Figure S6). Significant correlations for the regional averages only exist for A_a over 1960–2013 in the east of the South China Sea, the East China Sea, and the south-east of Japan ($R = 0.69, 0.39$ and 0.29 , respectively).

When $\eta - \eta_{IB}$ and η_{ster} from SODA during 1900–2010 are being used, the interannual variability of the seasonal amplitudes between the two sea level components is significantly correlated in most areas, except in

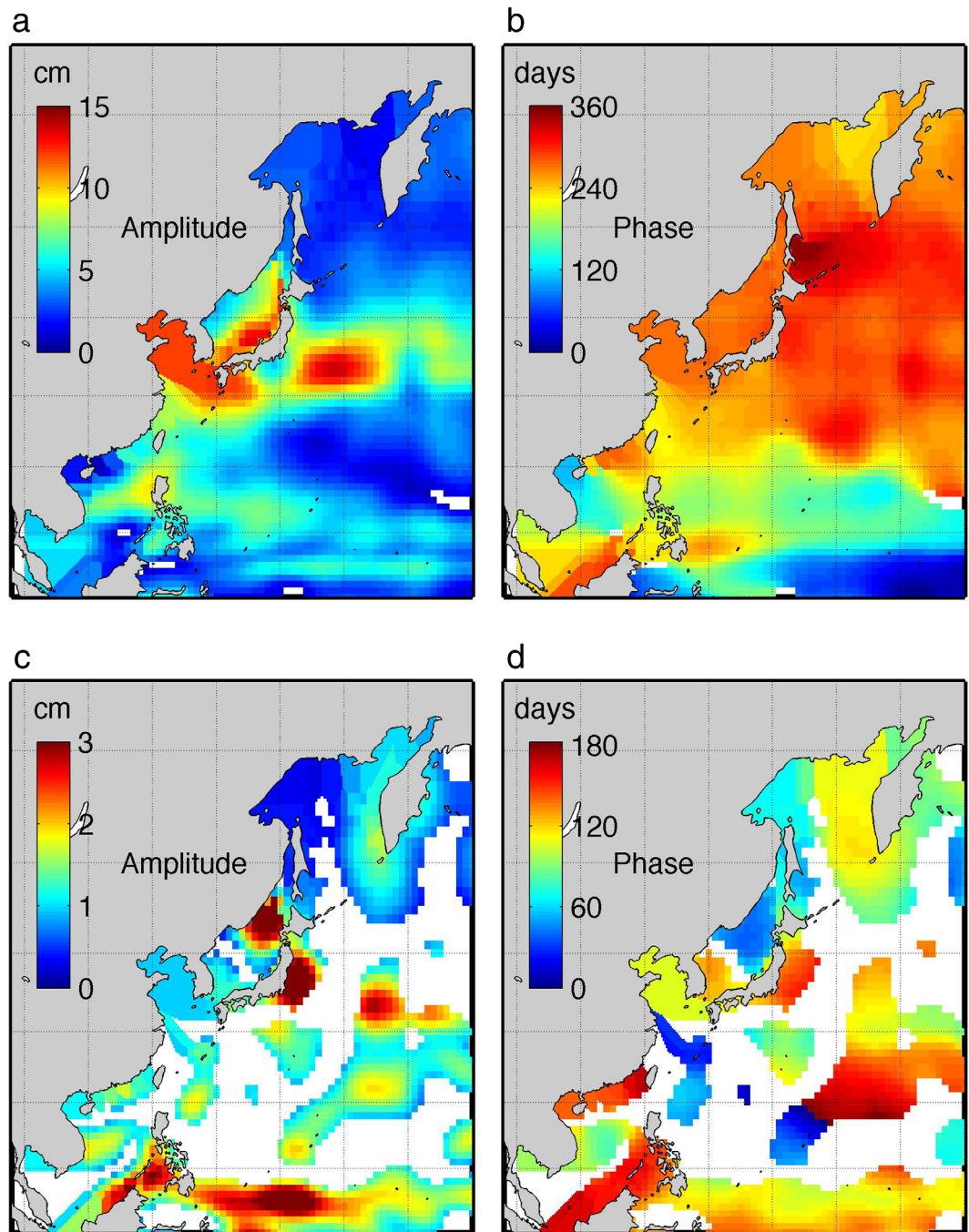


Figure 7. Mean (a) A_a , (b) ϕ_a , (c) A_{sa} , and (d) ϕ_{sa} for η_{ster} derived from EN4 over 1993–2013. Blank areas indicate the estimates of the annual or semiannual cycle parameters that are not passing the significance test at 95% confidence level. Please note that the scales of amplitudes here are different from those in Figure 3.

the Sea of Okhotsk. η_{ster} explains more than 80% of interannual variations of A_a in $\eta-\eta_{IB}$ in the open ocean and the central South China Sea (Figure 8). At the coastal regions, the relationships between η_{ster} and $\eta-\eta_{IB}$ at seasonal scales become weak but still significant (at 95% confidence level), where η_{ster} explains 5–30% of interannual variability of A_a in $\eta-\eta_{IB}$. The relationships at the coastal regions are different from the un-robust correlations recognized between the tide gauge records and EN4 data (above paragraph). This inconsistency can be partly attributed to the fact that EN4 is an interpolated product which means that the steric values at a single point over the slope are the result of integrating observations from the shelf as well as from the open ocean. This is not the case in an ocean model, in which every single point is representative

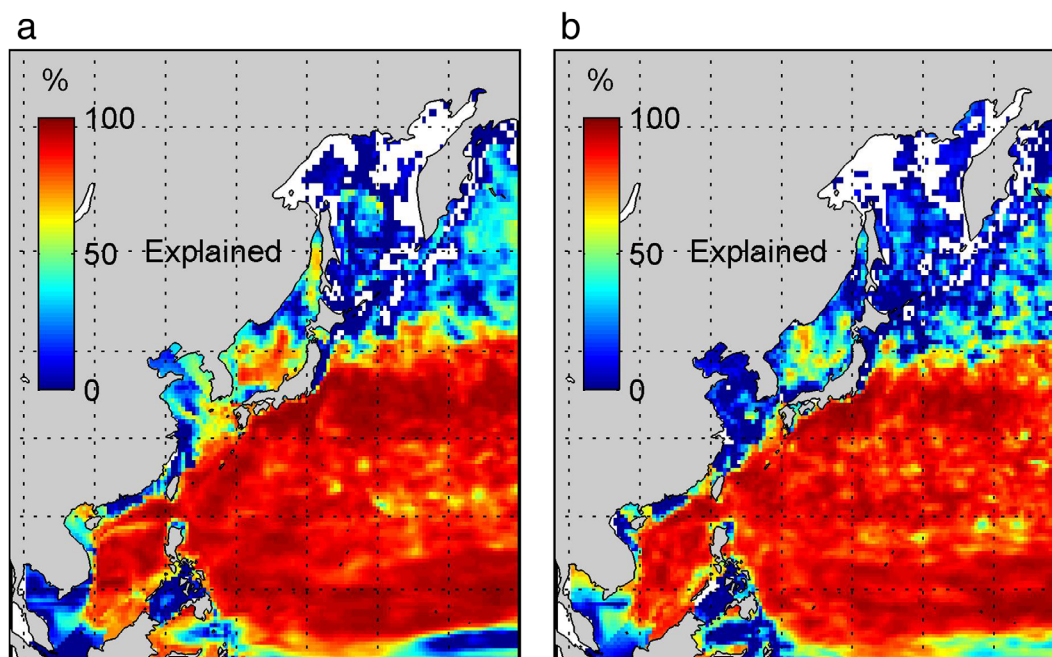


Figure 8. Percentage of the interannual variability of (a) A_a and (b) A_{sa} for $\eta\text{-}\eta_{IB}$ explained by that of η_{ster} over 1900–2010, derived from SODA. Blank areas indicate the grids where the correlation of the interannual variability of A_a or A_{sa} between $\eta\text{-}\eta_{IB}$ and η_{ster} are not significant at 95% confidence level.

of the variability on its own location. On top of this, the length of tide gauge records may also have an impact, as they are always shorter than the SODA reanalysis (111 years). Furthermore, it is also possible that SODA misses some processes that are recorded by tide gauges. What we can confirm at this moment from the two different assessments is that the contribution of η_{ster} to the interannual variations of the seasonal sea level cycle along the coasts is not as robust as that in the open ocean.

4.1.3. Residuals

Removing η_{IB} and η_{ster} from the observed η permits the sea level residuals, $\eta\text{-}\eta_{IB}\text{-}\eta_{ster}$, which have significantly reduced A_a in the East China Sea, the Sea of Japan, the Luzon Strait and the open ocean, and at 89 of the 120 tide gauge records (Figure 9a). We recall here that η_{ster} is appointed as the values at the closest grid points over the continental slope (500 m deep). However, the annual cycle of $\eta\text{-}\eta_{IB}\text{-}\eta_{ster}$ remains significant in most marginal seas and at 114 of the 120 tide gauge records. A_a with values of 5–10 cm are found in the East China Sea, the Sea of Okhotsk, and spots of the Kuroshio Extension region. It is worth noting that the removal of η_{IB} and η_{ster} increases A_a by 5–10 cm in the west of the South China Sea. This confirms the finding by Ponte [2006] that η_{IB} has a negative contribution to the monthly sea level variance in the Southeast Asia. ϕ_a of $\eta\text{-}\eta_{IB}\text{-}\eta_{ster}$ varies gradually in each marginal sea, but more heterogeneous features are found in the open ocean where A_a is low (Figure 9b).

The semiannual cycle of $\eta\text{-}\eta_{IB}\text{-}\eta_{ster}$ is still significant at 98 tide gauge stations and in most areas of marginal seas (Figures 9c and 9d). Removal of η_{IB} and η_{ster} has limited influence on the semiannual cycle in the marginal seas, except in the Sea of Japan and the east of the Sea of Okhotsk. In these two areas, A_{sa} increases by 2–4 cm when the two effects are subtracted. The existence of the seasonal cycle in $\eta\text{-}\eta_{IB}\text{-}\eta_{ster}$ indicates other mechanisms, beside η_{IB} and η_{ster} , to force the seasonal sea level cycle (e.g., wind effects). Of course, we cannot rule out the possibility that $\eta\text{-}\eta_{IB}\text{-}\eta_{ster}$ estimated here might be influenced by the limitations of the data set EN4 that is used to determine η_{ster} .

4.2. Impacts From the Wind Stress and the Sea Surface Currents

As mentioned above, η_{IB} and η_{ster} cannot fully explain the whole budgets of the observed seasonal sea level cycle either in its mean values or its interannual variability, especially in the marginal seas. Therefore, in this subsection we explored the potential contributions of the wind stress and the sea surface currents by correlating the long-term seasonal cycle amplitudes. The wind stress is expected to alter sea level variations via

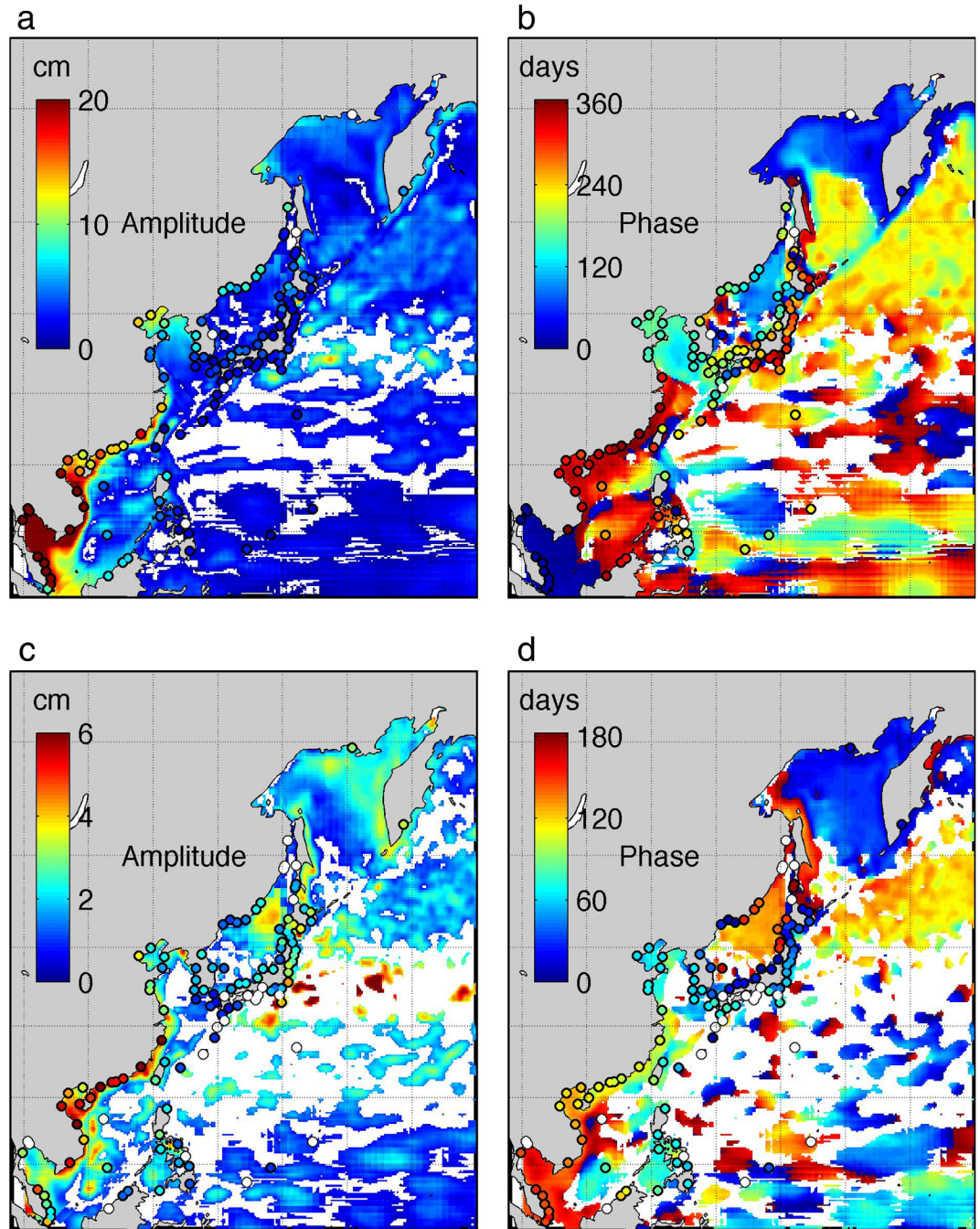


Figure 9. Mean (a) A_a , (b) ϕ_a , (c) A_{sa} , and (d) ϕ_{sa} for $\eta - \eta_{IB} - \eta_{ster}$ when η_{IB} and η_{ster} are removed from η provided by tide gauges and AVISO. Blank circles and areas indicate the estimates of the annual or semiannual cycle parameters that are not passing the significance test at 95% confidence level.

the mechanisms of ocean upwelling/downwelling in coastal regions and water piling at the equator, which are caused by the alongshore winds and the trade winds, respectively, through the Ekman transport [Segar, 2007]. In the open ocean, the vertical Ekman pumping due to the wind stress curl is able to produce the sea level variations as well, especially for the steric component because of the thermocline changes. The geostrophic balance is responsible for the mechanisms behind the links between sea level and horizontal sea surface currents. We performed the analyses in the seasonal cycle of $\eta - \eta_{IB}$ and $\eta - \eta_{IB} - \eta_{ster}$ to distinguish the impacts of the two contributors on different components of sea level. The interannual variability of A_a and A_{sa} for the wind stress and the sea surface currents with different directions over 1900–2010 was calculated

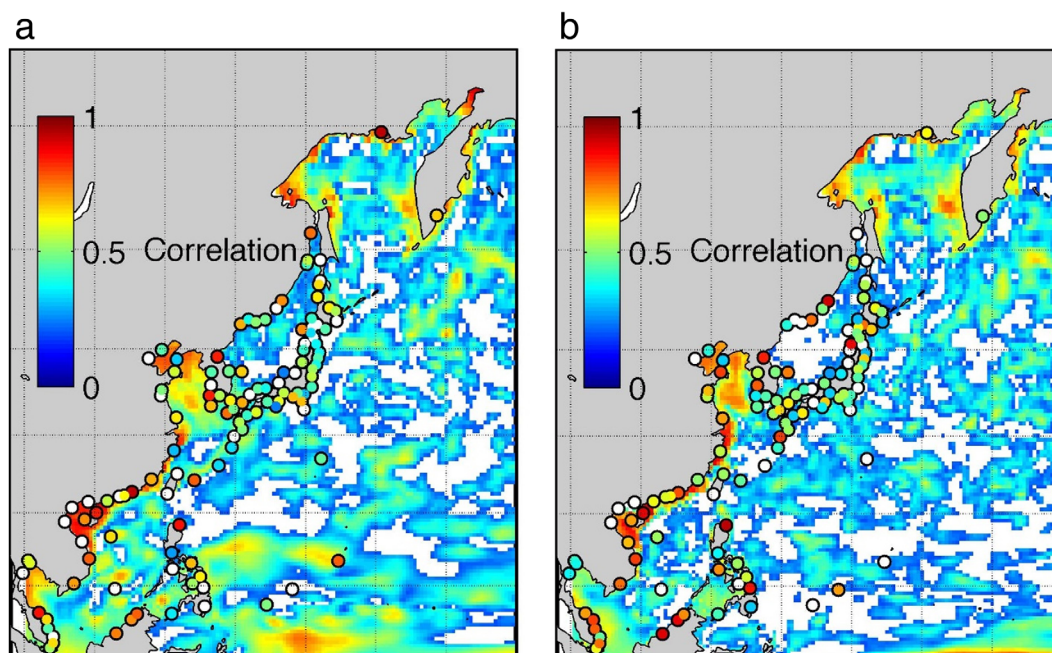


Figure 10. (a) Best correlation coefficients of the interannual variability of A_a between $\eta - \eta_{IB}$, provided by tide gauges and SODA, and the nearby wind stress; (b) same as (a), but for the correlations between $\eta - \eta_{IB} - \eta_{ster}$ and the nearby wind stress. Blank circles and areas indicate the correlations that do not pass the significance test at 95% confidence level. Note that the direction of wind stress corresponding to the best correlation coefficients is provided in supporting information Figure S7.

as mentioned in subsection 2.5. Because AVISO records (21 years) are not long enough to fully resolve the decadal changes in the seasonal sea level cycle and SODA, on the other hand, is able to reasonably reproduce the seasonal sea level cycle (as indicated in subsection 2.4), we used the sea surface height $\eta - \eta_{IB}$ from SODA over the period 1900–2010 in this subsection instead, along with the observed $\eta - \eta_{IB}$ from tide gauges over the same period.

4.2.1. Wind Stress

The best correlations of the inter-annual variability of A_a in $\eta - \eta_{IB}$ with that in different directions of wind stress nearby (with 1° radius around the location of sea level data) over 1900–2010 are shown in Figure 10a. The correlation coefficient is significant (at 95% confidence level) at 90 of the 120 tide gauge records and in most areas of the marginal seas. High correlations ($R = 0.6$ – 0.9) are found in the tropics and in the west areas of marginal seas. The direction of wind stress that corresponds to the best correlations with sea level is provided in supporting information (supporting information Figure S7). In the western areas of marginal seas, the annual cycle of sea level is better correlated with the zonal wind stress, while in the north Japan and the open ocean it is better correlated with the meridional wind stress component.

The regional averages of the interannual variability of A_a for tide gauge records are well correlated with the corresponding quantity for the wind stress (Figure 11a), with $R = 0.58, 0.48, 0.59, 0.33, 0.48,$ and 0.41 over 1960–2010 for the six subregions from south to north, respectively. A_a of sea level is changing by about 2 cm for every 10^{-2} N/m^2 of changes in A_a of the wind stress for the regional averages.

When η_{ster} is removed, the correlation of A_a between sea level and wind stress remains nearly unchanged in the shallow waters of most marginal seas (Figure 10b), except in the west of the Sea of Japan. This means that the temporal variations of the annual sea level cycle are dominated by $\eta - \eta_{IB} - \eta_{ster}$ and this component is well related to the local wind. This identification could be interpreted as the results of the coastal upwelling/downwelling or the wind-driven sea surface currents in the coastal areas. Figure 10 also shows that when η_{ster} is excluded the relationship of sea level with wind stress disappears in the central of the Sea of Japan, the central of the South China Sea, and the tropics. The annual cycle in η_{ster} over these areas can then be interpreted as wind stress-dependent. This might be caused by the vertical Ekman pumping and the equatorial upwelling that are both closely associated with the wind stress and that are both significant for modulating the steric height.

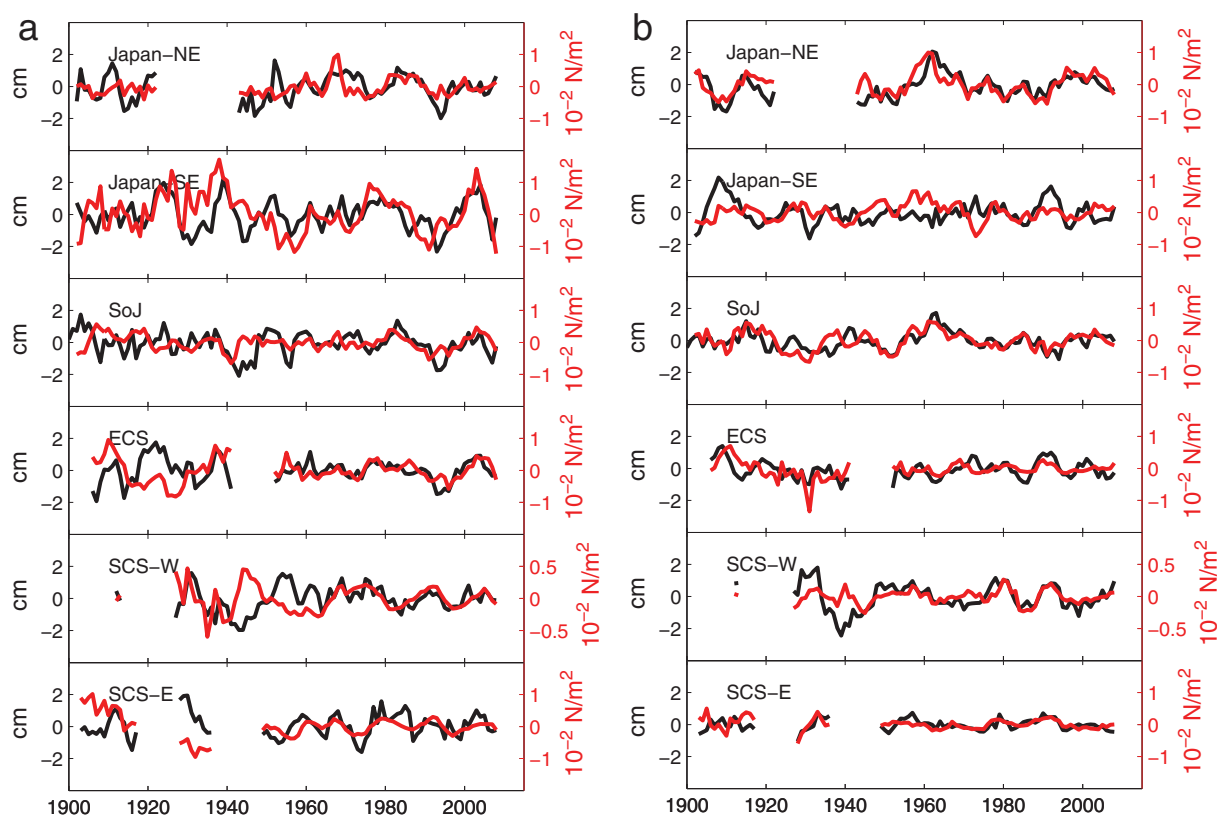


Figure 11. Time series of regional average anomaly of (a) A_a and (b) A_{sa} for $\eta-\eta_{IB}$ (black) against the corresponding average of the wind stress (red) in six subregions as specified in Figure 1.

The semiannual sea level cycle has significant correlations with nearby wind stress at 99 of the 120 tide gauge records and in large areas of marginal seas as well (not shown here). The best agreements for A_{sa} between sea level observations and the wind stress are in the northeast coasts of Japan and the west coasts of the South China Sea (Figure 11b). Similarly as revealed in the annual sea level cycle, the subtraction of η_{ster} does not apparently change the correlations with the wind stress for A_{sa} in the marginal seas.

4.2.2. Sea Surface Currents

The best correlations of the interannual variability of A_a between $\eta-\eta_{IB}$ and the sea surface currents nearby are presented in Figure 12a. The correlation is significant at 117 of the 120 tide gauge records and in most areas. The relationships are stronger than those with the wind stress in most areas. Higher correlations ($R = 0.7-0.95$) appear in the regions where the ocean currents are known to be strong, such as the Oyashio and Kuroshio Currents regions [Hurlburt *et al.*, 1996] and the Luzon Strait [Xue *et al.*, 2004]. The direction of the sea surface currents that is allocated to the best correlations with sea level varies regionally except in subtropical areas where the associations seem to be more determined by the meridional currents (supporting information Figure S8). The fast changes of the surface current direction for the best correlations indicate that the geostrophic response of sea level might be acting locally and at small scales. Also, we are aware that our method may not work well if the current direction for the best correlations is changing in time. This limitation may cause fast changes in the identified direction of the surface currents as well.

The regional averages of A_a anomalies of sea level from tide gauge observations correlate well with the changes in the surface currents, with $R=0.63, 0.45, 0.82, 0.71, 0.69$ and 0.62 over 1960–2010 for the six subregions from south to north respectively (Figure 13a). The regression for A_a is approximately 2 cm of increase in sea level for 1 cm/s increase in the current speed. However, this scale is greatly reduced prior to 1960 when the surface currents have larger range of variations (Figure 13a). This is due to the fact that the magnitude of the geostrophic response of sea level to nearby surface currents varies with locations (see supporting information Figure S9) presumably because of topography changes and thus the calculation of regional averages using fewer individual records prior to 1960 (Figure 1b) leads to the average values that reflect more localized features rather than the regional average features.

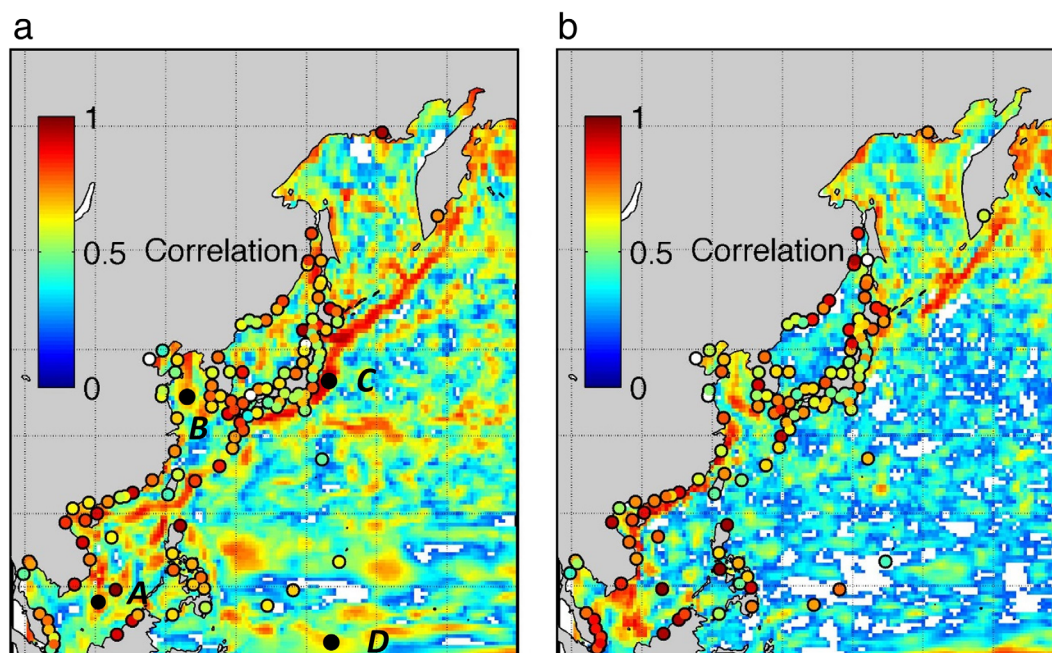


Figure 12. Same as Figure 10, but for best correlations with the nearby sea surface currents. Black dots in (a) highlight four grid points: A [8°N, 108°E], B [38°N, 123°E], C [37°N, 143°E], and D [4°N, 143°E]. Note that the direction of surface currents corresponding to the best correlation coefficients with sea level is provided in supporting information Figure S8.

When η_{ster} is excluded from $\eta - \eta_{IB}$, A_a of sea level is still highly dependent on the surface currents at 117 of the 120 tide gauge records, in the shallow waters of marginal seas and in the north of the Oyashio Current region (Figure 12b). This indicates that in these areas $\eta - \eta_{IB} - \eta_{ster}$ dominates the relationships of $\eta - \eta_{IB}$ with the surface currents due to the geostrophic balance as expected. This can be further evidenced by comparing the time series of A_a in η_{ster} and in $\eta - \eta_{IB} - \eta_{ster}$ with the corresponding quantity in the surface currents at specific points (Figures 14a and 14b). At location A [8°N, 108°E] in the Gulf of Thailand, the interannual variability of A_a in η_{ster} , the dominating component in sea level, is significantly correlated with the variability of the local surface current ($R = 0.78$). In contrast, changes in η_{ster} have no links with the current ($R = 0.1$, not significant at 95% confidence level). When location B [38°N, 123°E] in the East China Sea is selected, A_a in η_{ster} becomes comparable to that in $\eta - \eta_{IB} - \eta_{ster}$. The surface current has a significant correlation with η_{ster} ($R = 0.23$), but it has an even stronger correlation with $\eta - \eta_{IB} - \eta_{ster}$ ($R = 0.45$).

However, the removal of η_{ster} eliminates the high correlations that are identified for sea level in the open oceans, particularly in the areas of the south Oyashio, the Kuroshio, and the North Equatorial Currents, and in the Luzon Strait (Figure 12). The disappearance of correlations in these areas implies that η_{ster} , as the dominating component of sea level in the open ocean, is firmly regulated by the surface currents. Time series of the variables at two locations in these areas are also plotted to support this argument (Figures 14c and 14d). At location C [37°N, 143°E] on the route of the Kuroshio Current, the temporal variations of A_a between η_{ster} and the surface current are very well matched ($R = 0.90$). At location D [4°N, 143°E] near to the North Equatorial Current, they are significantly correlated as well but with a reduced correlation coefficient ($R = 0.33$).

It is worth noticing that the surface currents and the wind stress used in the analysis cannot be independent. The interannual variability of their seasonal cycles shows significant correlations in the marginal seas (except in the Sea of Japan) and in the tropics, with $R = 0.7$ – 0.95 (see supporting information Figure S10). Thus, the relationships of sea level with the surface currents that are found in the marginal seas and in the tropics (Figure 12) could be thought to be the consequence of the impact from the local wind. However, no significant correlations between the surface currents and the wind stress are found in the open ocean, particularly in the regions with the strong currents, where no robust correlations are found between sea level and the wind stress either (Figure 10). Therefore, the high correlations of sea level with the surface currents in these areas can be further interpreted as the consequence of the geostrophic balance between η_{ster} and the large-scale ocean currents, which are not forced by the local wind field.

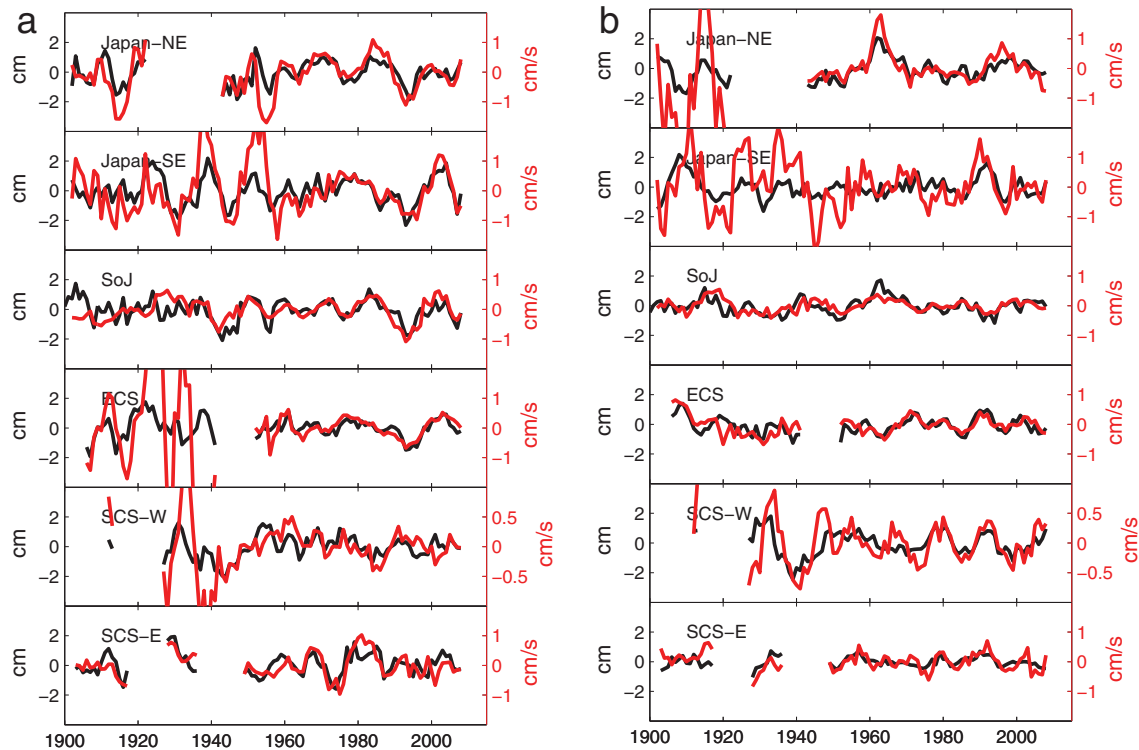


Figure 13. Same as Figure 11, but for time series of the sea surface currents (red).

The changes in A_{sa} of sea level are significantly correlated with the changes in the surface currents at 117 tide gauge records and in most areas (not shown here). The results for the regional averages of tide gauge records are shown in Figure 13b. The correlations are again better than those obtained from the wind stress.

5. Conclusions

The spatial and temporal features of the seasonal sea level variations in the northwest Pacific have been described by investigating the sea level observations from tide gauges (1900–2013) and gridded altimetry product AVISO (1993–2013). In the marginal seas, 60–95% of the monthly sea level variance can be explained by the annual and semiannual cycles, except in the Sea of Okhotsk where the seasonal sea level variance is weak and sea ice becomes important [Parkinson *et al.*, 1999]. However, in the open ocean and especially in eddy-rich regions (e.g., the Kuroshio Extension and the Oyashio Current) where the monthly sea level is mainly driven by the mesoscale eddies, the regular seasonal oscillations only account for 3–20% of the observed sea level variance.

The annual sea level cycle is significant over the whole area of study, with A_a over 10 cm in the East China Sea, the Luzon Strait, the Gulf of Thailand, and the Kuroshio Current regions. The largest A_a of ~ 30 cm is observed in the north of the East China Sea. The semiannual sea level cycle is only significant along the coasts and in the shallow waters of most marginal seas. The largest A_{sa} is ~ 6 cm on the northwestern coasts of the South China Sea. The seasonal cycle parameters of sea level estimated from tide gauge records and AVISO were compared. At the sites closest to tide gauge stations, AVISO significantly underestimates A_a by 2–9 cm (25%) at 59 of 120 stations and A_{sa} by 1–3 cm (60%) at 28 stations. The discrepancies mainly occur on the coasts of China and Russia.

The contributions of the IB effect (η_{IB}) and the steric height (η_{ster}) to the observed seasonal sea level cycle have been identified. η_{IB} has significant impact on the annual sea level cycle over the whole area of study, which causes the largest A_a of 12 cm in the East China Sea. The semiannual cycle of η_{IB} is only significant at

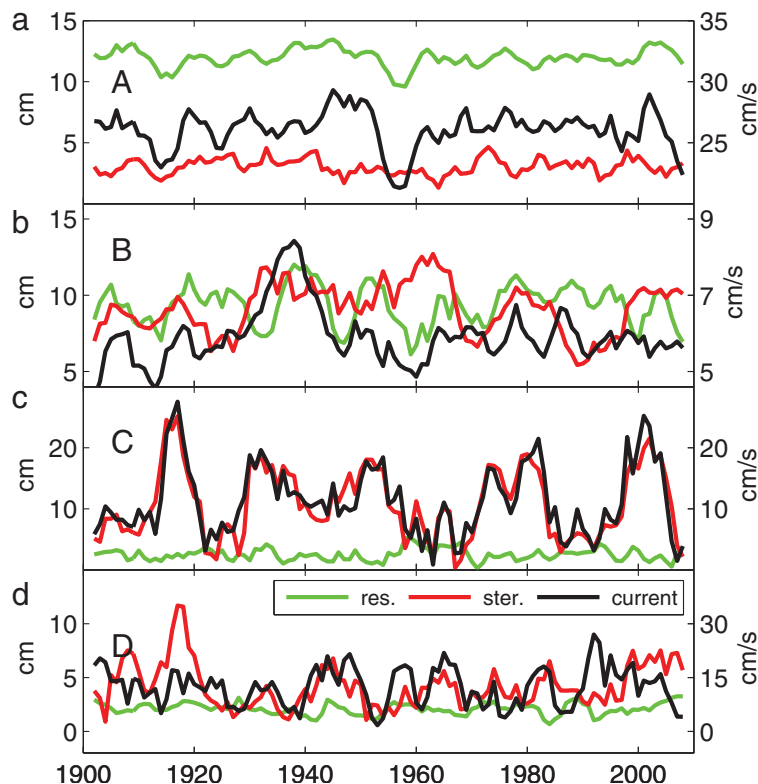


Figure 14. Time series of A_a for $\eta - \eta_{IB} - \eta_{ster}$ (green) and η_{ster} (red), along with the corresponding quantity of the sea surface currents that are best corrected with time series for $\eta - \eta_{IB}$, at 4 grid points A-D (a-d) as indicated in Figure 12a.

the central north Pacific where A_{sa} is ~ 3 cm. η_{ster} , mainly due to the thermal expansion of seawater, can produce A_a with up to 8–12 cm in the East China Sea, the east of Sea of Japan, and the Kuroshio Extension region. The removal of η_{IB} and η_{ster} significantly diminishes the annual sea level cycle in most areas, but increases the annual cycle by 5–10 cm in the west of the South China Sea. The removal has little impact on the semiannual cycle. Significant seasonal cycles still remain in the residuals over the marginal seas.

The long-term tide gauge observations allow us to assess the temporal variability of the seasonal sea level variations on the coasts. The annual and semiannual sea level cycles are not stable with time, with amplitudes changing between 2–20.4 cm and 1–7 cm, respectively. η_{IB} and η_{ster} have limited influences on the observed interannual variability of the seasonal sea level cycle based on our analysis. However, in the open ocean η_{ster} explains over 80% of interannual variations based on ocean reanalysis of SODA.

The dynamic forcing of the interannual variability in the seasonal sea level cycle was also diagnosed using SODA data. The wind stress and especially the sea surface currents are correlated with the seasonal sea level cycle at most tide gauge records and in the marginal seas, as the consequence of their strong contributions to the sea level residuals. The regional averages of the seasonal cycle amplitudes are changing by ~ 2 cm for 10^{-2} N/m² and 1 cm/s changes in the amplitudes of the wind stress and the surface currents, respectively. Because in the marginal seas and in the tropics the seasonal variations of the currents are highly dependent on the local wind stress, the relationships of sea level with the surface currents observed here can be interpreted as the consequence of the wind-driven Ekman transport. In the open ocean, especially in the regions of the western boundary currents, the surface currents can better describe the seasonal sea level variations ($R = 0.7$ – 0.95) than the wind stress, and this is mainly due to the significant associations between the steric height and the open ocean currents through the geostrophic equilibrium. However, there are still some areas in the open ocean, where neither the wind stress nor the surface currents can well explain the forcing of the seasonal steric height variations which account for over 80% of sea level changes. The vertical Ekman pumping caused by the wind stress curl might be the reason and we will work on this in the future.

Acknowledgments

This research is funded by Lloyd's Register Foundation, which supports the advancement of engineering-related education, and funds research and development that enhances safety of life at sea, on land and in the air. This work is also funded by the UK Natural Environment Research Council, which supports the work of X. Feng (in part), M. N. Tsimplis, F. M. Calafat and P. Cipollini at the National Oceanography Centre. X. Feng and J. Zheng appreciate the National Science Fund for Distinguished Young Scholars (grant 51425901). G. Jordà and M. Marcos acknowledge two Ramón y Cajal contracts funded by the Spanish Ministry of Economy and the Regional Government of the Balearic Islands. Tide gauge data used in the paper were obtained from the Permanent Service for Mean Sea Level (www.psmsl.org), and gridded satellite altimeter sea level records and DAC data were retrieved from AVISO (www.aviso.altimetry.fr). The ocean objective analyses EN4.0.2 were collected from the UK Met Office Hadley Centre (www.metoffice.gov.uk/hadobs/en4), and the wind stress, the sea surface currents and the reanalysis of other oceanic data were collected from SODA developed by Texas A&M University (<http://soda.tamu.edu>). The sea level pressure was retrieved from the NOAA's 20th century reanalysis and the ECMWF-Interim. We thank all these institutions for making their data publicly available, as well as three reviewers for their constructive comments and suggestions.

References

- Amiruddin, A. M., I. D. Haigh, M. N. Tsimplis, F. M. Calafat, and S. Dangendorf (2015), The seasonal cycle and variability of sea level in the South China Sea, *J. Geophys. Res. Oceans*, *120*, 5490–5513, doi:10.1002/2015JC010923.
- Anderson, C. J., and B. G. Lockaby (2012), Seasonal patterns of river connectivity and saltwater intrusion in tidal freshwater forested wetlands, *River Res. Appl.*, *28*, 814–826, doi:10.1002/rra.1489.
- Barbosa, S. M., M. E. Silva, and M. J. Fernandes (2008), Changing seasonality in North Atlantic coastal sea level from the analysis of long tide gauge records, *Tellus Ser. A*, *60*, 165–177, doi:10.1111/j.1600-0870.2007.00280.x.
- Bingham, R. J., and C. W. Hughes (2012), Local diagnostics to estimate density-induced sea level variations over topography and along coastlines, *J. Geophys. Res.*, *117*, C01013, doi:10.1029/2011JC007276.
- Boyer, T. P., et al. (2009), *World Ocean Database 2009, NOAA Atlas NESDIS 66*, edited S. Levitus, 216 pp., U.S. Gov. Print. Off., Washington, D. C.
- Carrère, L., and F. Lyard (2003), Modeling the barotropic response of the global ocean to atmospheric wind and pressure forcing: Comparisons with observations, *Geophys. Res. Lett.*, *30*(6), 1275, doi:10.1029/2002GL016473.
- Carton, J. A., and B. S. Giese (2008), A reanalysis of ocean climate using Simple Ocean Data Assimilation (SODA), *Mon. Weather Rev.*, *136*(8), 2999–3017, doi:10.1175/2007MWR1978.1.
- Carton, J. A., G. Chepurin, X. Cao, and B. Giese (2000), A simple ocean data assimilation analysis of the global upper ocean 1950–95. Part I: Methodology, *J. Phys. Oceanogr.*, *30*(2), 294–309, doi:10.1175/1520-0485(2000)030<0294:ASODAA>2.0.CO;2.
- Chelton, D. B., M. G. Schlax, and R. M. Samelson (2011), Global observations of nonlinear mesoscale eddies, *Progr. Oceanogr.*, *91*, 167–216.
- Chen, J. L., C. K. Shum, C. R. Wilson, D. P. Chambers, and B. D. Tapley (2000), Seasonal sea level change from TOPEX/Poseidon observation and thermal contribution, *J. Geod.*, *73*(12), 638–647, doi:10.1007/s001900050002.
- Compo, G., et al. (2011), The twentieth century reanalysis project, *Q. J. R. Meteorol. Soc.*, *137*(654), 1–28, doi:10.1002/qj.776.
- Dangendorf, S., C. Muddersbach, J. Jensen, G. Anette, and H. Heinrich (2013a), Seasonal to decadal forcing of high water level percentiles in the German Bight throughout the last century, *Ocean Dyn.*, *63*(5), 533–548, doi:10.1007/s10236-013-0614-4.
- Dangendorf, S., T. Wahl, C. Muddersbach, and J. Jensen (2013b), The Seasonal mean sea level cycle in the Southeastern North Sea, *J. Coastal Res.*, Special Issue No. 65, 1915–1920.
- Feng, X., and M. N. Tsimplis (2014), Sea level extremes at the coasts of China, *J. Geophys. Res. Oceans*, *119*, 1593–1608, doi:10.1002/2013JC009607.
- Feng, X., M. N. Tsimplis, and P. L. Woodworth (2015), Nodal variations and long-term changes in the main tides on the coasts of China, *J. Geophys. Res. Oceans*, *120*, 1215–1232, doi:10.1002/2014JC010312.
- Gabler, R., J., Petersen, L., Trapasso, and D., Sack (2008), *Physical Geography*, 9th ed., 672 pp., Cengage Learning, Belmont, USA.
- Giese, B. S., and S. Ray (2011), El Niño variability in simple ocean data assimilation (SODA), 1871–2008, *J. Geophys. Res.*, *116*, C02024, doi:10.1029/2010JC006695.
- Gill, A. E. (1982), *Atmosphere-Ocean Dynamics*, vol. 30, Academic Press, London, U. K.
- Good, S. A., M. J. Martin, and N. A. Rayner (2013), EN4: Quality controlled ocean temperature and salinity profiles and monthly objective analyses with uncertainty estimates, *J. Geophys. Res. Oceans*, *118*, 6704–6716, doi:10.1002/2013JC009067.
- Haines, K., M. Valdivieso, H. Zuo, and V. N. Stepanov (2012), Transports and budgets in a 1/4° global ocean reanalysis 1989–2010, *Ocean Sci.*, *8*, 333–344, doi:10.5194/os-8-333-2012.
- Hamlington, B. D., R. R. Leben, R. S. Nerem, W. Han, and K.-Y. Kim (2011), Reconstructing sea level using cyclostationary empirical orthogonal functions, *J. Geophys. Res. Oceans*, *116*, C12015, doi:10.1029/2011JC007529.
- Hamlington, B. D., R. R. Leben, L. A. Wright, and K.-Y. Kim (2012), Regional sea level reconstruction in the Pacific ocean, *Mar. Geod.*, *35*(sup1), 98–117, doi:10.1080/01490419.2012.718210.
- Han, G., and W. Huang (2008), Pacific decadal oscillation and sea level variability in the Bohai, Yellow, and East China seas, *J. Phys. Oceanogr.*, *38*(12), 2772–2783, doi:10.1175/2008JPO3885.1.
- Holgate, S. J., et al. (2013), New data systems and products at the permanent service for mean sea level, *J. Coastal Res.*, *29*(3), 493–504, doi:10.2112/JCOASTRES-D-12-00175.1.
- Hünicke, B., and E. Zorita (2008), Trends in the amplitude of Baltic Sea level annual cycle, *Tellus Ser. A*, *60*, 154–164, doi:10.1111/j.1600-0870.2007.00277.x.
- Hurlburt, H. E., A. J. Wallcraft, W. J. Schmitz Jr., P. J. Hogan, and E. J. Metzger (1996), Dynamics of the Kuroshio/Oyashio current system using eddy-resolving models of the North Pacific Ocean, *J. Geophys. Res.*, *101*(C1), 941–976, doi:10.1029/95JC01674.
- Kang, S. K., M. G. G. Foreman, H.-J. Lie, J.-H. Lee, J. Cherniawsky, and K.-D. Yum (2002), Two-layer tidal modeling of the Yellow and East China Seas with application to seasonal variability of the M₂ tide, *J. Geophys. Res.*, *107*(C3), 3020, doi:10.1029/2001JC000838.
- Marcos, M., and M. N. Tsimplis (2007), Variations of the seasonal sea level cycle in southern Europe, *J. Geophys. Res.*, *112*, C12011, doi:10.1029/2006JC004049.
- Marcos, M., M. N. Tsimplis, and F. M. Calafat (2012), Inter-annual and decadal sea level variations in the north-western Pacific marginal seas, *Progr. Oceanogr.*, *105*, 4–21, doi:10.1016/j.pcean.2012.04.010.
- Michael, H. A., A. E. Mulligan, and C. F. Harvey (2005), Seasonal oscillations in water exchange between aquifers and the coastal ocean, *Nature*, *436*(7054), 1145–1148, doi:10.1038/nature03935.
- Müller, M., J. Cherniawsky, M. Foreman, and J.-S. von Storch (2014), Seasonal variation of the M₂ tide, *Ocean Dyn.*, *64*(2), 159–177, doi:10.1007/s10236-013-0679-0.
- Parkinson, C. L., D. J. Cavalieri, P. Gloersen, H. J. Zwally, and J. C. Comiso (1999), Arctic sea ice extents, areas, and trends, 1978–1996, *J. Geophys. Res.*, *104*(C9), 20,837–20,856, doi:10.1029/1999JC900082.
- Pascual, A., M. Marcos, and D. Gomis (2008), Comparing the sea level response to pressure and wind forcing of two barotropic models: Validation with tide gauge and altimetry data, *J. Geophys. Res.*, *113*, C07011, doi:10.1029/2007JC004459.
- Passaro, M., P. Cipollini, and J. Benveniste (2015), Annual sea level variability of the coastal ocean: The Baltic Sea-North Sea transition zone, *J. Geophys. Res. Oceans*, *120*, 3061–3078, doi:10.1002/2014JC010510.
- Plag, H.-P., and M. N. Tsimplis (1999), Temporal variability of the seasonal sea-level cycle in the North Sea and Baltic Sea in relation to climate variability, *Global Planet. Change*, *20*, 173–203, doi:10.1016/S0921-8181(98)00069-1.
- Ponte, R. M. (2006), Low-frequency sea level variability and the inverted barometer effect, *J. Atmos. Oceanic Technol.*, *23*(4), 619–629, doi:10.1175/JTECH1864.1.
- Pugh, D., and P. Woodworth (2014), *Sea-Level Science: Understanding Tides, Surges, Tsunamis and Mean Sea-Level Changes*, 395 pp., Cambridge Univ. Press, Cambridge, U. K.
- Segar, D. A. (2007), *Introduction to Ocean Sciences*, 720 pp., W. W. Norton and Company, Inc., N. Y.

- Smith, R. D., J. K. Dukowicz, and R. C. Malone (1992), Parallel ocean general circulation modeling, *Physica D*, *60*(1), 38–61, doi:10.1016/0167-2789(92)90225-C.
- Tabata, S., B. Thomas, and D. Ramsden (1986), Annual and interannual variability of steric sea level along line P in the northeast Pacific Ocean, *J. Phys. Oceanogr.*, *16*(8), 1378–1398, doi:10.1175/1520-0485(1986)016<1378:AAIVOS>2.0.CO;2.
- Tamisiea, M. E., E. M. Hill, R. M. Ponte, J. L. Davis, I. Velicogna, and N. T. Vinogradova (2010), Impact of self-attraction and loading on the annual cycle in sea level, *J. Geophys. Res.*, *115*, C07004, doi:10.1029/2009JC005687.
- Torres, R. R., and M. N. Tsimplis (2012), Seasonal sea level cycle in the Caribbean Sea, *J. Geophys. Res.*, *117*, C07011, doi:10.1029/2012JC008159.
- Torres, R. R., and M. N. Tsimplis (2014), Sea level extremes in the Caribbean Sea, *J. Geophys. Res. Oceans*, *119*, 4714–4731, doi:10.1002/2014JC009929.
- Tsimplis, M. N., and A. G. P. Shaw (2010), Seasonal sea level extremes in the Mediterranean Sea and at the Atlantic European coasts, *Nat. Hazards Earth Syst. Sci.*, *10*, 1457–1475, doi:10.5194/nhess-10-1457-2010.
- Tsimplis, M. N., and P. L. Woodworth (1994), The global distribution of the seasonal sea level cycle calculated from coastal tide gauge data, *J. Geophys. Res.*, *99*(C8), 16,031–16,039, doi:10.1029/94JC01115.
- UNESCO (1981), Tenth Report of the International oceanographic Tables, *UNESCO Tech. Pap. Mar. Sci.*, *36*, 25 pp., Paris, France.
- Vignudelli S., A. G. Kostianoy, P. Cipollini, and J. Benveniste (Eds.) (2011), *Coastal Altimetry*, 578 pp., Springer, Berlin, doi:10.1007/978-3-642-12796-0.
- Vinogradov, S. V., and R. M. Ponte (2010), Annual cycle in coastal sea level from tide gauges and altimetry, *J. Geophys. Res.*, *115*, C04021, doi:10.1029/2009JC005767.
- Vinogradov, S. V., R. M. Ponte, P. Heimbach, and C. Wunsch (2008), The mean seasonal cycle in sea level estimated from a data-constrained general circulation model, *J. Geophys. Res.*, *113*, C03032, doi:10.1029/2007JC004496.
- Wahl, T., F. M. Calafat, and M. E. Luther (2014), Rapid changes in the seasonal sea level cycle along the US Gulf coast from the late 20th century, *Geophys. Res. Lett.*, *41*, 491–498, doi:10.1002/2013GL058777.
- Wang, W., H. Liu, Y. Li, and J. Su (2014), Development and management of land reclamation in China, *Ocean Coastal Manage.*, *102*, 415–425, doi:10.1016/j.ocecoaman.2014.03.009.
- Woodruff, S. D., et al. (2011), ICOADS Release 2.5: Extensions and enhancements to the surface marine meteorological archive, *Int. J. Climatol.*, *31*, 951–967, doi:10.1002/joc.2103.
- Wu, Z., E. K. Schneider, B. P. Kirtman, E. S. Sarachik, N. E. Huang, and C. J. Tucker (2008), The modulated annual cycle: an alternative reference frame for climate anomalies, *Clim. Dyn.*, *31*(7–8), 823–841, doi:10.1007/s00382-008-0437-z.
- Wunsch, C., and D. Stammer (1997), Atmospheric loading and the oceanic “inverted barometer” effect, *Rev. Geophys.*, *35*(1), 79–107, doi:10.1029/96RG03037.
- Xue, H., F. Chai, N. Pettigrew, D. Xu, M. Shi, and J. Xu (2004), Kuroshio intrusion and the circulation in the South China Sea, *J. Geophys. Res.*, *109*, C02017, doi:10.1029/2002JC001724.
- Yashayaev, I. M. and I. I. Zveryaev (2001), Climate of the seasonal cycle in the North Pacific and the North Atlantic oceans, *Int. J. Climatol.*, *21*, 401–417, doi:10.1002/joc.585.